Euro. Jnl of Applied Mathematics (2014), *vol.* 25, *pp.* 83–115.
doi:10.1017/S0956792513000314

Coarsening rates for the dynamics of slipping droplets

GEORGY KITAVTSEV

Max-Planck Institute for Mathematics in the Sciences, Inselstraße 22, 04103 Leipzig, Germany
email: georgy.kitavtsev@mis.mpg.de

(*Received 13 July 2013; revised 30 July 2013; accepted 2 August 2013; first published online 4 September 2013*)

Reduced ordinary differential equation (ODE) models arising from a high-order lubrication system and describing coarsening dynamics of droplets in nanometric polymer film interacting on a hydrophobically coated solid substrate in the presence of large slippage at the liquid/solid interface are analysed. In the limiting case of infinite slip length corresponding in applications to free films, a collision/absorption model then arises and is solved explicitly. The exact coarsening law is derived for it analytically and confirmed numerically. Existence of a threshold for the decay of initial distributions of droplet distances at infinity at which the coarsening rates switch from algebraic to exponential ones is shown.

Key words: Coarsening rates; Wall slippage; Droplet collisions; Absorption model; Lubrication equations; Free films; Asymptotic analysis

1 Introduction

Dewetting processes of a liquid polymer film of nanometer thickness interacting on a hydrophobically coated solid substrate have attracted intensive research during last several decades, see. e.g. [4, 10, 33]. In general, such processes can be divided into three stages. During the first stage a liquid polymer film is susceptible to instability due to small perturbations of film profile. Typically, such films rupture, thereby initiating a complex dewetting process, see e.g. [37, 38, 40]. The influence of intermolecular forces plays an important part in the rupture and subsequent dewetting process, see e.g. [11, 42 and references therein]. Typically, the competition between the long-range attractive and short-range repulsive van der Waals forces reduces the unstable film to *an ultrathin layer* that connects evolving patterns and is given by the minimum of the corresponding intermolecular potential, i.e. the film settles into an energetically more favourable state, see [3, 14]. The second stage is associated with the formation of regions of this minimal thickness, bounded by moving rims that connect to the undisturbed film, see e.g. [8, 31, 41].

In this study we are interested in the third and the last stages of the dewetting process, namely the long-time coarsening process that originates in the breaking up of the evolving patterns into small droplets and is characterized by its subsequent slow-time coarsening dynamics, which has been observed and investigated experimentally by Limary and Green [25, 26]. They show that during coarsening the average size of droplets increases and the number of droplets decreases. The coarsening mechanisms that were

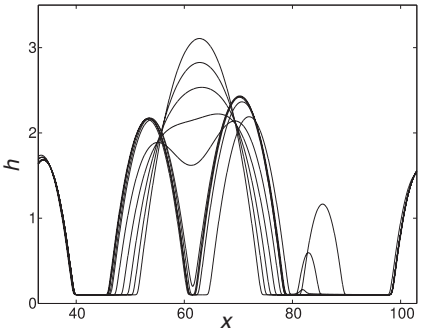

FIGURE 1. Numerical solution to (1.5a)–(1.5b) with $\varepsilon = 0.1$, $\beta = 2.5$, $\mathrm{Re} = 1$, $\sigma = 1$, $v = 4$ showing an example of a coarsening process (collapse of the 4th small droplet and collision of the 2nd and 3rd droplets) in *an array* of five quasi-equilibrium droplets.

observed in such films are typically subsequent collapses of smaller droplets and collisions of neighbouring ones. During collapse the size of a droplet shrinks in time and its mass is distributed in the ultrathin layer. In turn, collisions among droplets occur due to the mass transfer through the ultrathin layer between them that causes a translation movement between them, i.e. *droplet migration*. Colliding droplets each time form a bigger droplet. A numerical example of coarsening dynamics in two-dimensional films is shown in Figure 1.

Besides intermolecular forces and surface tension at the free surface of the film, the dewetting of polymer films on hydrophobic substrates also involves such boundary effect as slippage on a solid substrate [6, 7, 15]. Recently, in Münch *et al.* [32] one-dimensional lubrication equations over a wide range of slip lengths were derived from the underlying equations for the conservation of mass and momentum, together with boundary conditions for tangential and normal stresses as well as the kinematic condition at the free boundary, impermeability and the Navier-slip condition at the liquid–solid interface. Asymptotic arguments based on the magnitude of the slip length show that within a lubrication scaling there are two *distinguished regimes*, see [32].

These are the *weak-slip* and *strong-slip* models. The former model was derived under the scaling of the physical slip-length B as $B = \eta b$, where the (small) parameter η, $0 < \eta \ll 1$, refers to the vertical to horizontal scale separation of thin film, and b denotes the non-dimensionalised slip length parameter. This model takes the form

$$\partial_t h = -\partial_x\Big((h^3 + b\,h^2)\partial_x\,(\sigma\partial_{xx}h - \Pi_\varepsilon(h))\Big). \tag{1.1}$$

Here $h(x,t)$ denotes the height profile for the free surface of a liquid film. The high order of the lubrication equation (1.1) is a result of the contribution from surface tension at the free boundary, reflected by the linearized curvature term $\sigma\partial_{xx}h$ with parameter $\sigma > 0$. Further contribution to the pressure is denoted by $\Pi_\varepsilon(h)$ and represents that of intermolecular forces, namely long-range attractive and short-range repulsive van der Waals intermolecular forces. Our analysis here can be applied to a general class of intermolecular potentials which includes those commonly employed to describe the

https://doi.org/10.1017/S0956792513000314 Published online by Cambridge University Press

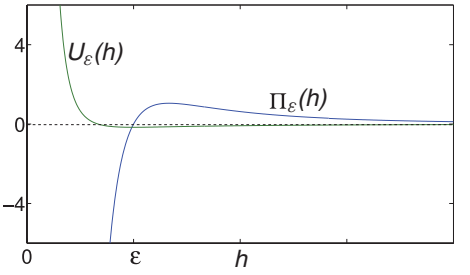

FIGURE 2. (Colour online) Plot of intermolecular pressure $\Pi_\varepsilon(h)$ and potential function $U_\varepsilon(h)$ for $\varepsilon = 0.1$.

dewetting in nanoscopic thin films [33]. A potential from this class should satisfy the following assumptions:

- It should have a unique zero at $0 < \varepsilon \ll 1$, and a unique maximum at $P_{\max}(\varepsilon)$.
- It should decay as $O(h^{-\alpha})$ for $h \to +\infty$ with some $\alpha > 3$ and tend to $-\infty$ as $h \to 0$.

For illustrative purposes we work below with a fixed potential from this class already used for the analysis of coarsening dynamics in [3, 18, 19] and given by

$$\Pi_\varepsilon(h) = \frac{\varepsilon^2}{h^3} - \frac{\varepsilon^3}{h^4} \quad \text{with} \quad 0 < \varepsilon \ll 1. \tag{1.2}$$

The corresponding maximum value in this case is given by

$$P_{\max}(\varepsilon) = \frac{27}{256\varepsilon}. \tag{1.3}$$

The potential can be written as a derivative of the potential function $U_\varepsilon(h) = \mathscr{U}(h/\varepsilon)$ (see Figure 2), where

$$\mathscr{U}(H) = -\frac{1}{2H^2} + \frac{1}{3H^3}. \tag{1.4}$$

The small parameter ε is the global minimum of $U_\varepsilon(h)$ and to the leading order gives the thickness of an ultrathin layer.

In turn, the *strong-slip* model describing the second important asymptotic regime was derived in [32] under the scaling of the physical slip-length B as $B = \beta/\eta$ and takes the form

$$\mathrm{Re}\,(\varepsilon\partial_t(hu) + \partial_x(hu^2)) = v\partial_x(h\partial_x u) + h\partial_x(\sigma\partial_{xx}h - \Pi_\varepsilon(h)) - \frac{u}{\beta}, \tag{1.5a}$$

$$\varepsilon\partial_t h = -\partial_x(hu), \tag{1.5b}$$

with β denoting the non-dimensionalised slip-length parameter in this case. Here $u(x,t)$ and $h(x,t)$ denote the average velocity in the lateral direction and the height profile for the free surface, respectively. Terms $\mathrm{Re}\,(\partial_t(hu) + \partial_x(hu^2))$ and $v\partial_x(h\partial_x u)$ in (1.5a)–(1.5b), with Re, $v \geqslant 0$ denoting the Reynolds number and viscosity parameter, represent inertial and Trouton viscosity terms, respectively. The pressure and the flux terms in this model

https://doi.org/10.1017/S0956792513000314 Published online by Cambridge University Press

have the form

$$p(h) = \sigma \partial_{xx} h - \Pi_\varepsilon(h), \quad j(h,u) = hu. \tag{1.6}$$

Note that the small parameter ε from the definition (1.2) is introduced as the prefactor before time derivatives in (1.5a)–(1.5b) in order to capture later on the right timescale for the slow dynamics associated with collapse and collisions of droplets.

In addition, the weak-slip and strong-slip models contain as limiting cases three further lubrication models. One of them is the *no-slip model*, which is obtained setting $b = 0$ in the weak-slip model:

$$\partial_t h = -\partial_x \Big(h^3 \partial_x \left(\partial_{xx} h - \Pi_\varepsilon(h) \right) \Big). \tag{1.7}$$

The second one is obtained from the strong-slip model in the limit $\beta \to \infty$ and describes the dynamics of suspended or falling free films:

$$\mathrm{Re}\left(\varepsilon \partial_t (hu) + \partial_x (hu^2)\right) = \nu \partial_x (h \partial_x u) + h \partial_x (\sigma \partial_{xx} h - \Pi_\varepsilon(h)), \tag{1.8a}$$

$$\varepsilon \partial_t h = -\partial_x (hu). \tag{1.8b}$$

For the third limiting case, the non-dimensionalised slip-length parameter β_I is taken of the order of magnitude of the physical slip-length B, therefore lying in between those that lead to the weak-slip and strong-slip models. The corresponding *intermediate-slip* model is given by (up to rescaling time by β_I)

$$\partial_t h = -\partial_x \Big(h^2 \partial_x \left(\partial_{xx} h - \Pi_\varepsilon(h) \right) \Big). \tag{1.9}$$

It can be obtained by rescaling time in (1.1) by b and letting $b \to \infty$ or by rescaling time and the horizontal velocity by β in (1.5a)–(1.5b) and taking the limit $\beta \to 0$. Existence of weak solutions in (1.5a)–(1.5b) and (1.8a)–(1.8b) and rigorous convergence of the former ones to the classical solutions of (1.9) as $\beta \to 0$ was shown recently in [22].

As in [22], we consider systems (1.5a)–(1.5b) and (1.8a)–(1.8b) on a bounded interval $(0, L)$ with the boundary conditions

$$u = 0, \quad \text{and} \quad \partial_x h = 0 \quad \text{at} \quad x = 0,\, L, \tag{1.10}$$

whereas equations (1.1), (1.7) and (1.9) with

$$\partial_{xxx} h = 0, \quad \text{and} \quad \partial_x h = 0 \quad \text{at} \quad x = 0,\, L. \tag{1.11}$$

Both (1.10) and (1.11) incorporate zero flux at the boundary and as a consequence imply the conservation of mass

$$\frac{1}{L} \int_0^L h(x,t)\, dx = \text{const}, \ \forall t > 0.$$

Within the context of thin liquid films, first studies of the coarsening dynamics can be found in Glasner and Witelski [18, 19] and Pismen and Pomeau [36]. There the authors considered the no-slip lubrication model (1.7). They confirmed numerically the existence of two coarsening driven mechanisms, namely collision and collapse. One of the typical problems considered in [18, 19] was the calculation of coarsening rates, i.e. how fast the

https://doi.org/10.1017/S0956792513000314 Published online by Cambridge University Press

number of droplets decreases due to coarsening in time. Often, in order to identify the characteristic dependence for coarsening rates one needs to model very large arrays of droplets (around 10^4). But due to the presence of the ultrathin layer of order ε between droplets, the problem of numerical solution for any lubrication equation becomes very stiff in time and demands high spatial resolution as the number of droplets increases. Therefore, there exists a need for further reduction of lubrication models to more simple, possibly finite-dimensional ones.

The authors in [18, 19] observed that solutions of lubrication equations describing coarsening dynamics stay in time very close to a perturbed finite combination of quasi-stationary droplets and can be therefore parameterized by a finite number of parameters, namely positions and pressures of drops. On the basis of this observation they derived for the first time from the lubrication equation (1.7) a closed reduced ODE model describing the slow evolution of positions and pressures in time. Using this reduced model the authors also derived the corresponding coarsening law in the form

$$n(t) \sim t^{-2/5}, \tag{1.12}$$

where $n(t)$ denotes the number of droplets remaining at time t. Later, analogous reduced ODE models from lubrication equation (1.1) with a general mobility $M(h) = h^q$, $q > 0$ in one- and two-dimensional cases were derived and analysed in [16, 17]. A step to rigorous justification of these models on the basis of a centre manifold approach was made recently in [23]. For the case $M(h) = h$ the coarsening law (1.12) was justified rigorously in [34] using the gradient flow structure of the corresponding lubrication equation. The works of [16, 17] concern the migration of droplet. There it was shown that the direction of the migration of droplets governed by (1.1) with a general mobility $M(h) = h^q$, $q > 0$ is opposite to one of the mass flux from the surrounding ultrathin film. Moreover, for $q \leqslant 2$ the driving coarsening mechanism is collapse of droplets that is due to mass diffusion in the ultrathin layer between droplets and is similar to Ostwald ripening in binary alloys, see [1, 2, 39]. Also note that in the no-slip case $q = 3$, i.e. one described by (1.7), as was shown in [19] even the systems coarsening solely due collisions obey the law (1.12).

Recently, Kitavtsev and Wagner [24] and Kitavtsev [21] have shown that the coarsening dynamics of quasi-stationary droplets governed by (1.5a)–(1.5b) is also driven by collapse and collision. There reduced ODE models analogous to that of [18, 19] were derived for system (1.5a)–(1.5b) as well as for its limiting case (1.8a)–(1.8b). In contrast to the case of (1.1), it was found there that the coefficients of the strong-slip reduced ODE model explicitly depend on the slip length β. In particular, there exists a critical length $\beta_{\mathrm{cr}} = O(\varepsilon)$ such that the migration of droplets proceeds in the direction of the applied mass flux for $\beta > \beta_{\mathrm{cr}}$ and opposite to it for $\beta < \beta_{\mathrm{cr}}$. Moreover, it was shown that for moderate and large β the driving coarsening mechanism switches from collapse to collision of droplets. Based on these observations it was conjectured and shown numerically in [24] that the coarsening rates for systems (1.5a)–(1.5b) and (1.8a)–(1.8b) can be remarkably different from (1.12).

In this study we continue the research initiated in [24]. Our aim here is to derive explicit coarsening laws for the dynamics of droplets in the strong-slip and free film regimes, i.e. governed by lubrication system (1.5a)–(1.5b) and its limiting case (1.8a)–(1.8b). The part

https://doi.org/10.1017/S0956792513000314 Published online by Cambridge University Press

missing in [24] was the derivation of flux representation between interacting droplets for moderate and large slip lengths β which was important for the closure of the derived reduced ODE models. Therefore, inspired by the matched asymptotics technique applied by Glasner [16] to the lubrication equation (1.1), we present in Section 2 a closed form derivation of reduced ODE models for (1.5a)–(1.5b) and (1.8a)–(1.8b) that incorporate the explicit flux representation for all $0 < \beta \leqslant \infty$.

In Section 3 we concentrate on the reduced ODE model corresponding to (1.8a)–(1.8b), i.e. on the regime of free films characterized by the infinite slip length $\beta = \infty$. In this case the migration and subsequent collisions of droplets dominate completely the collapse events during the coarsening process. Therefore, we look only at the migration subsystem of the derived reduced ODE model such that droplet masses and accordingly (as it is explained in detail in Section 3) pressures are kept constant during evolution of droplets and updated only after each subsequent collision event. We further observe that for special initial data this migration subsystem can be explicitly solved, while its solution represents subsequent collisions of $N-1$ droplets with the largest last one. Therefore, we call such combination of the migration ODEs and the initial data an exactly solvable collision/absorption model. It turns out that the coarsening law for this model depends only on the initial distribution of distances between droplets and can be derived analytically. Finally, we derive the continuous counterpart of the coarsening law proceeding to the limit $N \to \infty$.

In Section 4 we consider several examples of initial distributions of distances between droplets and show that the corresponding coarsening rates depend only on the distribution decay at infinity. Moreover, for an explicit family of distributions decaying as $1/x^{1+\alpha}$ with $\alpha > 0$, we show the existence of a threshold at $\alpha = 1$ at which the coarsening rates switch from algebraic to exponential ones.

In Section 5.1 we justify the derived hierarchy of the reduced models by the numerical comparison of their solutions with the solutions of the initial partial differential equation (PDE) system (1.5a)–(1.5b) and its limiting cases (1.9) and (1.5a)–(1.5b). We observe that deviation between them stays $O(\varepsilon)$ uniformly in time. Next, we compare solutions of the collision/absorption model from Section 3 with those of a fully reduced ODE system for the case $\beta = \infty$. Finally, in Section 5.2 we check numerically the derived coarsening law for the collision/absorption model in the case of finite N and its continuous counterpart.

2 Derivation of reduced ODE models

We consider a solution to (1.5a)–(1.5b) which stays close in time to a union of $N+1$ droplets, whose precise characterization is described below. Similar to the derivation of reduced coarsening models for the classical thin film equation in [16], we distinguish three regions in our matched asymptotic analysis (see Figure 3).

- *Droplet core (DC) region*: This region corresponds to droplets and is composed of the union of disjoint intervals $(X_i(t) - R_i(t), X_i(t) + R_i(t))$ so that $X_i(t)$ and $R_i(t)$ are respectively the centre and the radius of the ith droplet, where $i = 0, \ldots, N$. The dynamical points $X_i(t) \pm R_i(t)$ are called contact line points and are defined through the

https://doi.org/10.1017/S0956792513000314 Published online by Cambridge University Press

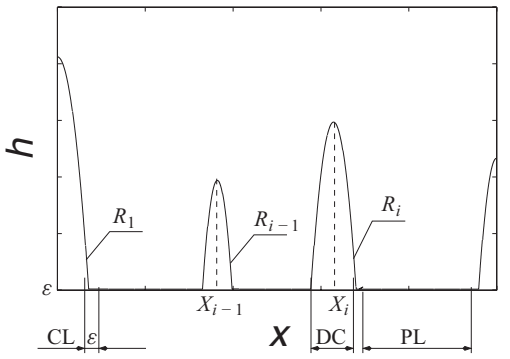

FIGURE 3. Three asymptotic regions in an array of droplets.

relation

$$h(X_i \pm R_i) = \varepsilon H^*, \tag{2.1}$$

where H^* is the global maximum of $U'(H)$ with function $U(H)$ defined in (1.4). We expand

$$R_i = R_{i,0} + \varepsilon R_{i,1} + \cdots, \quad X_i = X_{i,0} + \varepsilon X_{i,1} + \cdots \tag{2.2}$$

and denote

$$\dot{R} = \frac{dR}{dt}, \quad \dot{X} = \frac{dX}{dt}.$$

- *Contact line (CL) region*: It is a microscopic internal layer in the neighbourhood of the contact line points where h and x scale like ε. Here we employ the change of variables $(x,t) \to (z,\tau)$, where z denotes the moving rescaled spatial coordinate, i.e

$$z = \frac{R(t) - |x - X(t)|}{\varepsilon}, \quad \mp\partial_x = \frac{1}{\varepsilon}\partial_z, \quad \partial_t = \partial_\tau - \frac{1}{\varepsilon}\partial_z(\dot{R}_0 \mp \dot{X}_0). \tag{2.3}$$

  Sign $\mp$ in the last expression corresponds to two CL regions around the points $X \mp R$, respectively. Accordingly, by definition (2.1) we have $h(z=0) = \varepsilon H^*$.

- *Precursor layer (PL) region*: It is the complement $(-L, L) \setminus \cup_i (X_i - R_i, X_i + R_i)$. In this region h scales like ε.

The main goal is to determine the evolution of $R_i(t)$ and $X_i(t)$. To do so as in [16], we propose self-consistent asymptotic expansions in each of the three regions and connect them via matching conditions as $\varepsilon \to 0$. Corrections to the leading order base solutions solve linear equations, and the Fredholm-type solvability conditions will yield information about the dynamics. Proceeding so, we consider other physical parameters $\mathrm{Re}, \beta, \sigma, \nu$ in (1.5a)–(1.5b) to be $O(1)$ as $\varepsilon \to 0$. We should point out that the asymptotical analysis below is valid for both the case of finite and zero Reynolds numbers Re. The corresponding inertia terms in (1.5a)–(1.5b) appear to be of much smaller order in the leading order and corrector equations as far as the following balance between Re and ε holds,

$$\mathrm{Re} \ll \varepsilon^{-2} \tag{2.4}$$

https://doi.org/10.1017/S0956792513000314 Published online by Cambridge University Press

and therefore do not influence the leading order of coarsening dynamics of droplets. Condition (2.4) is consistent with physical parameter balances used during the derivation of (1.5a)–(1.5b) in [32].

2.1 Leading order systems

Let us first consider the motion of the ith droplet with $i \in 1,\dots,N-1$. For the convenience in this and next two sections, we suppress the subscript i. Let us start with the CL region. Here the solution to (1.5a)–(1.5b) is expanded as

$$h = \varepsilon H_1 + \varepsilon^2 H_2 + \cdots, \quad u = \varepsilon U_1 + \varepsilon^2 U_2 + \cdots$$

We will also use the induced expansions

$$P = P_0 + \varepsilon P_1 + \cdots, \quad J = \varepsilon^2 J_2 + \varepsilon^3 J_3 + \cdots$$

for the pressure and flux functions defined in (1.6). The corresponding leading order system in ε in this region is given by

$$\begin{aligned} &\partial_z(\sigma \partial_{zz} H_1 - U'(H_1)) = 0,\\ &\partial_z H_1(\dot{R}_0 \mp \dot{X}_0) = \mp \partial_z(H_1 U_1). \end{aligned}$$

Integrating the last system and using matching conditions to the DC and PL regions

$$\begin{aligned} \partial_z H_1 \to 0,\ \partial_{zz} H_1 \to 0, H_1 \to 1 \text{ as } \ z \to -\infty,\\ \partial_{zz} H_1 \to 0,\ H_1 \to +\infty \text{ as } \ z \to +\infty, \end{aligned} \tag{2.5}$$

one obtains

$$\frac{\sigma}{2}(\partial_z H_1)^2 = U(H_1) - U(1), \tag{2.6a}$$

$$U_1 = -(1 - \frac{1}{H_1})(\dot{R}_0 \mp \dot{X}_0) \mp \frac{J_2(-\infty)}{H_1}. \tag{2.6b}$$

In particular,

$$\lim_{z\to+\infty} U_1 = -(\dot{R}_0 \mp \dot{X}_0), \quad \lim_{z\to-\infty} U_1 = \mp J_2(-\infty). \tag{2.7}$$

Next, in the DC region we expand the solution as

$$h = h_0 + \varepsilon h_1 + \varepsilon^2 h_2 + \cdots, \quad u = u_0 + \varepsilon u_1 + \varepsilon^2 u_2 + \cdots$$

and correspondingly pressure as

$$p = p_0 + \varepsilon p_1 + \cdots$$

In turn, the leading order system in this region is given by

$$\begin{aligned} \sigma h_0 \partial_x(\partial_{xx} h_0) - \frac{u_0}{\beta} = 0,\\ -\partial_x(h_0 u_0) = 0. \end{aligned}$$

https://doi.org/10.1017/S0956792513000314 Published online by Cambridge University Press

Integrating the second equation in the last system and using the matching condition

$$h_0(X \mp R) = 0 \tag{2.8}$$

one obtains $u_0 \equiv 0$. Next, integrating the first equation one obtains the full solution

$$h_0 = \frac{1}{R\sqrt{12\sigma}}(R^2 - (x - X(t))^2), \quad u_0 \equiv 0. \tag{2.9}$$

Correspondingly, the leading order pressure is given by

$$p_0 \equiv \frac{1}{R\sqrt{3\sigma}}. \tag{2.10}$$

In the PL region we expand the solution as

$$h = \varepsilon h_1 + \varepsilon^2 h_2 + \cdots, \quad u = \varepsilon u_1 + \varepsilon^2 u_2 + \cdots$$

and correspondingly pressure and flux as

$$p = p_0 + \varepsilon p_1 + \cdots, \quad j = \varepsilon^2 j_2 + \varepsilon^3 j_3 + \cdots$$

The leading order system in this region is given by

$$\begin{aligned} h_1 \partial_x(U'(h_1)) &= 0, \\ \partial_t h_1 &= -\partial_x(h_1 u_1). \end{aligned}$$

Integrating the system and using the matching condition $h_1(X \mp R) = 1$, one obtains

$$h_1 \equiv 1, \quad u_1 = j_2 \equiv \text{const.} \tag{2.11}$$

2.2 Corrector systems in PL and CL regions

For the next order corrections h_2, u_2 in the PL region, one has the system

$$\begin{aligned} h_1 \partial_x(U''(h_1)h_2) &= -\frac{u_1}{\beta}, \\ \partial_t h_2 &= -\partial_x(h_1 u_2 + h_2 u_1). \end{aligned}$$

From the first equation and (2.11) one obtains

$$\partial_{xx} h_2 = \partial_{xx} p_0 = 0 \quad \text{and} \quad j_2 = -\beta \partial_x p_0. \tag{2.12}$$

Proceeding further in the expansion in the CL region for the second-order corrections H_2, U_2, one obtains the system

$$\begin{aligned} -v\partial_z(H_1 \partial_z U_1) &= H_1(\sigma \partial_{zz} H_2 - U''(H_1)H_2), \\ 0 &= \partial_z H_2(\dot{R}_0 - \dot{X}_0) - \partial_z(H_1 U_2 + H_2 U_1). \end{aligned} \tag{2.13}$$

https://doi.org/10.1017/S0956792513000314 Published online by Cambridge University Press

Let us introduce a linear operator

$$\mathscr{L}\begin{bmatrix} H \\ U \end{bmatrix} = \begin{bmatrix} H_1\partial_z(\sigma\partial_{zz}H_2 - U''(H_1)H_2)) \\ \partial_z(H_2(\dot{R}_0 - \dot{X}_0 - U_1) - H_1U_2) \end{bmatrix}.$$

The formal adjoint operator to $\mathscr{L}$ is given by

$$\mathscr{L}^*\begin{bmatrix} g \\ v \end{bmatrix} = \begin{bmatrix} -\sigma\partial_{zzz}(H_1g) + U''(H_1)\partial_z(H_1g) - \partial_z V(\dot{R}_0 - \dot{X}_0 - U_1) \\ \partial_z v H_1 \end{bmatrix}.$$

The following two linear independent functions lie in the kernel of the operator $\mathscr{L}^*$:

$$\begin{bmatrix} g_1 \\ v_1 \end{bmatrix} := \begin{bmatrix} 1 \\ 0 \end{bmatrix}, \quad \begin{bmatrix} g_2 \\ v_2 \end{bmatrix} := \begin{bmatrix} 1/H_1 \\ 0 \end{bmatrix}. \tag{2.14}$$

To derive necessary Fredholm-type solvability conditions for the system (2.13) we multiply the first equation in (2.13) by g_2 and integrate it by $(-\infty, +\infty)$ to obtain

$$P_0(+\infty) - P_0(-\infty) = \int_{-\infty}^{+\infty} \frac{v}{H_1}\partial_z(H_1\partial_z U_1)\,dz,$$

where we have used that in the CL region

$$P_0 = U''(H_1)H_2 - \sigma\partial_{zz}H_2. \tag{2.15}$$

Substituting in the previous expression (2.6b), one obtains

$$P_0(+\infty) - P_0(-\infty) = -vI(\mp J_2(-\infty) + \dot{R}_0 \mp \dot{X}_0), \tag{2.16}$$

where a constant integral I is given by

$$I = \int_{-\infty}^{+\infty} \frac{1}{H_1}\partial_z\left(\frac{\partial_z H_1}{H_1}\right) dz = \frac{1}{35(3+\sqrt{3})}, \tag{2.17}$$

and can be effectively calculated from (2.6a) (see Appendix A). Formula (2.16) is an analog of the Gibbs–Thomson boundary condition and shows that the pressure experiences a jump at the CL region. Note that this is the first considerable difference between the coarsening dynamics driven by (1.5a)–(1.5b) and (1.1). In contrast to (2.16), as was shown in [18], the pressure is constant through the CL region in the case of (1.1).

Next, multiplying the first equation in (2.13) by g_3 and integrating it on $(-\infty, +\infty)$ one obtains

$$0 = vH_1\partial_z U_1\Big|_{-\infty}^{+\infty} + \int_{-\infty}^{+\infty} H_1\partial_z(\sigma\partial_{zz}H_2 - U''(H_1)H_2)\,dz.$$

Integrating further three times by parts and using (2.6b) and (2.15) one arrives at

$$0 = -v\frac{\partial_z H_1}{H_1}(\mp J_2(-\infty) + \dot{R}_0 \mp \dot{X}_0)\Big|_{-\infty}^{+\infty} - H_1P_0\Big|_{-\infty}^{+\infty}$$

$$- \sigma\partial_z H_1\partial_z H_2\Big|_{-\infty}^{+\infty} + \sigma\partial_{zz}H_1H_2\Big|_{-\infty}^{+\infty},$$

https://doi.org/10.1017/S0956792513000314 Published online by Cambridge University Press

Using the matching condition (2.5) and in addition

$$\begin{aligned}&\partial_z H_2 \to \text{const as } \; z \to -\infty,\\ &\partial_z H_1 \to \partial_x h_0,\ \partial_z H_2 \sim \partial_x h_1 + \partial_{xx} h_0 z,\ H_1 \sim h_1 + \partial_x h_0 z \text{ as } \; z \to +\infty,\end{aligned} \tag{2.18}$$

one arrives at

$$(H_1 P_0)\Big|_{-\infty}^{+\infty} = \sigma \partial_z H_1(+\infty)\partial_z H_2(+\infty).$$

The last expression again using (2.5) and (2.18) implies

$$\begin{aligned}\sigma \partial_{xx} h_0 &= -P(+\infty),\\ \sigma(\partial_x h_0 \partial_x h_1)\Big|_{X \mp R} &= P(-\infty) - P(+\infty) h_1(X \mp R).\end{aligned} \tag{2.19}$$

Note that the first relation in (2.19) is consistent with already derived (2.9)–(2.10), whereas the second one is new.

2.3 Corrector system in the DC region

Finally, let us consider the system for the first-order corrections h_1, u_1 in the DC region which has the form

$$0 = v\partial_x(h_0 \partial_x u_1) + \sigma h_0 \partial_{xxx} h_1 - u_1/\beta, \tag{2.20a}$$

$$\frac{\partial h_0}{\partial R}\dot{R}_0 - \frac{\partial h_0}{\partial x}\dot{X}_0 = -\partial_x(h_0 u_1). \tag{2.20b}$$

Similarly, we again introduce a linear operator

$$\mathscr{L}\begin{bmatrix} h \\ u \end{bmatrix} = \begin{bmatrix} v\partial_x(h_0 \partial_x u_1) + \sigma h_0 \partial_{xxx} h_1 - u_1/\beta \\ -\partial_x(h_0 u_1) \end{bmatrix}.$$

The formal adjoint operator to $\mathscr{L}$ is given by

$$\mathscr{L}^*\begin{bmatrix} g \\ v \end{bmatrix} = \begin{bmatrix} v\partial_x(h_0 \partial_x g) - \frac{g}{\beta} + h_0 \partial_x v \\ -\sigma \partial_{xxx}(h_0 g) \end{bmatrix}.$$

The following two linear independent functions lie in the kernel of the operator $\mathscr{L}^*$:

$$\begin{bmatrix} g_1 \\ v_1 \end{bmatrix} := \begin{bmatrix} 0 \\ 1 \end{bmatrix}, \quad \begin{bmatrix} g_2 \\ v_2 \end{bmatrix} := \begin{bmatrix} 1 \\ \int_X^x \frac{d\tau}{\beta h_0} \end{bmatrix}. \tag{2.21}$$

To derive the necessary Fredholm-type solvability conditions for the system (2.20a)–(2.20b) we multiply (2.20b) by v_1, integrate it and using the matching condition (2.8) obtain

$$\dot{R}_0 = 0. \tag{2.22}$$

https://doi.org/10.1017/S0956792513000314 Published online by Cambridge University Press

In turn, multiplying the right-hand side of the second equation in (2.13) by v_2 and integrating it by $(X-R, X+R)$, one obtains

$$0 = -\dot{X}_0 \int_{X-R}^{X+R} \frac{\partial h_0}{\partial x} v_2 \, dx + \int_{X-R}^{X+R} \partial_x (h_0 u_1) v_2 \, dx = h_0 u_1 v_2 \Big|_{X-R}^{X+R} - \int_{X-R}^{X+R} h_0 u_1 \partial_x v_2 \, dx$$
$$- \dot{X}_0 \int_{X-R}^{X+R} \frac{\partial h_0}{\partial x} v_2 \, dx = \dot{X}_0 (h_0 v_2) \Big|_{X-R}^{X+R} - \frac{2\dot{X}_0 R}{\beta} - \frac{1}{\beta} \int_{X-R}^{X+R} u_1 \, dx$$
$$= -\frac{2\dot{X}_0 R}{\beta} - \frac{1}{\beta} \int_{X-R}^{X+R} u_1 \, dx.$$

In the last equality we used that $h_0 \sim O(R - |x - X|)$ and $v_2 \sim \log(R - |x - X|)$ as $x \to X \mp R$. Next, using (2.20a) and integrating three times by parts, one arrives at

$$\frac{2\dot{X}_0 R}{\beta} = -\frac{1}{\beta} \int_{X-R}^{X+R} u_1 \, dx = \int_{X-R}^{X+R} v \partial_x (h_0 \partial_x u_1) + \sigma h_0 \partial_{xxx} h_1 \, dx$$
$$= \left[v h_0 \partial_x u_1 + \sigma h_0 \partial_{xx} h_1 - \sigma \partial_x h_0 \partial_x h_1 + \sigma \partial_{xx} h_0 h_1 \right] \Big|_{X-R}^{X+R}. \tag{2.23}$$

Let us note that from (2.20a)–(2.20b) and (2.22) and (2.8) it follows that

$$u_1 \equiv \dot{X}_0, \tag{2.24a}$$
$$\partial_{xxx} h_1 = \frac{\dot{X}_0}{\beta \sigma h_0}. \tag{2.24b}$$

Hence, by (2.24a) the first term in the square brackets in (2.23) vanishes. By (2.24b) one has $\partial_{xx} h_1 \sim \log(R - |x - X|)$ as $x \to X \pm R$. Due to this and (2.8)–(2.9) the second term in the square brackets in (2.23) also vanishes. In turn, due to the matching condition

$$h_1(X \mp R) = H_1(0) \tag{2.25}$$

and (2.9), the fourth fourth term in the square brackets in (2.23) vanishes. Therefore, relation (2.23) reduces to

$$\frac{2\dot{X}_0 R}{\beta} = -\left[\sigma \partial_x h_0 \partial_x h_1 \right] \Big|_{X-R}^{X+R}. \tag{2.26}$$

2.4 The final form of the reduced ODE system

At this moment let us introduce back the droplet subscript $i = 1, \ldots, N-1$. In this section as in (2.2), the first subscript points out to the droplet label whereas the second one points to the corresponding term in the asymptotic expansion. Denote by J_i the flux j_2 in the PL region between $i-1$th and ith droplets. Combining (2.12) with (2.16) and (2.22) one obtains that J_i is constant and satisfies

$$J_i = \beta \frac{P_i - P_{i-1} - 2v J_i I - v I (\dot{X}_{i,0} + \dot{X}_{i-1,0})}{d_i}. \tag{2.27}$$

https://doi.org/10.1017/S0956792513000314 Published online by Cambridge University Press

In the last formula we introduced two more notations: the constant leading order pressure inside ith droplet

$$P_i = \frac{1}{R_i\sqrt{3\sigma}} \tag{2.28}$$

according to (2.10), and the distance between the neighbouring DC regions

$$d_i = X_i - X_{i-1} - R_i - R_{i-1}.$$

From (2.27) one obtains an explicit expression for J_i:

$$J_i = \beta \frac{P_i - P_{i-1} - vI(\dot{X}_{i,0} + \dot{X}_{i-1,0})}{d_i + 2vI\beta}, \quad i = 1, \ldots, N. \tag{2.29}$$

Next, from (2.26), the matching conditions (2.19) and (2.25) and equations (2.16) and (2.22) one obtains the leading order equation for ith droplet position evolution

$$\dot{X}_{i,0} = -\frac{I\beta v}{2R_i + 2I\beta v}(J_{i+1} + J_i).$$

Substituting in the last expression the flux representation (2.29), denoting

$$\widetilde{d}_i = \frac{d_i}{Iv\beta}, \tag{2.30}$$

and using (2.28) one obtains

$$\dot{X}_{i,0} = -\frac{P_i}{2/(\sqrt{3\sigma}\beta) + 2IvP_i}\left(\frac{(P_{i+1} - P_i) - Iv(\dot{X}_{i+1} + \dot{X}_i)}{\widetilde{d}_{i+1} + 2} + \frac{(P_i - P_{i-1}) - Iv(\dot{X}_i + \dot{X}_{i-1})}{\widetilde{d}_i + 2}\right),$$

$$\text{for} \quad i = 1, \ldots, N-1. \tag{2.31}$$

In turn by (2.22) and definition (2.28) one has

$$\dot{P}_{i,0} = 0, \quad \text{for} \quad i = 0, \ldots, N.$$

The derived ODE system describing the leading order in ε evolution of pressures and positions of $N+1$ droplets will be closed if we additionally prescribe that the first and the last droplet do not move, i.e

$$\dot{X}_{0,0} = \dot{X}_{N,0} = 0, \; X_0 = 0, \; X_N = L. \tag{2.32}$$

The condition (2.32) corresponds to the situation when one extends the array on $N+1$ droplets from interval $(0, L)$ to an infinite array on the whole real line $\mathbb{R}$ by reflection around the points $x = 0$ and $x = L$. It also stays in agreement with boundary conditions (1.10) and (1.11).

Let us point out that the evolution of pressures is slower than one of the positions and proceeds on the order ε. One can potentially obtain it by going further in the expansion of the solution to (1.5a)–(1.5b), while an easier way is to derive it from the conservation of droplet volume as was done in [16,18] for the case of equation (1.1). Namely, the volume

https://doi.org/10.1017/S0956792513000314 Published online by Cambridge University Press

of the ith droplet V_i is changing due to the difference of the fluxes in the PL regions surrounding it. Using (2.9) and (2.28), one obtains

$$\dot{V}_{i,0} = \varepsilon \frac{4}{3\left(\sqrt{3\sigma}P\right)^3}\dot{P}_{i,1} = \varepsilon^2(J_{i+1} - J_i). \tag{2.33}$$

Substituting in the last expression the flux representation (2.29) and denoting

$$C_i = \varepsilon \frac{3\left(\sqrt{3\sigma}P\right)^3}{4},$$

one obtains

$$\varepsilon\dot{P}_{i,1} = \frac{C_i}{Iv}\left(\frac{P_{i+1}-P_i}{\widetilde{d}_{i+1}+2} - \frac{P_i - P_{i-1}}{\widetilde{d}_i+2}\right) - C_i\left(\frac{\dot{X}_{i+1}-\dot{X}_i}{\widetilde{d}_{i+1}+2} - \frac{\dot{X}_i - \dot{X}_{i-1}}{\widetilde{d}_i+2}\right),\ i = 1,\ldots,N-1.$$

Finally, combining the last expression with (2.31) and (2.32) and omitting higher order terms in ε, the closed ODE system for the leading order evolution of positions and pressures in array of $N+1$ droplets takes the following form:

$$\dot{X}_i = -\frac{P_i}{2/(\sqrt{3\sigma}\beta) + 2IvP_i}\left(\frac{(P_{i+1}-P_i) - Iv(\dot{X}_{i+1}+\dot{X}_i)}{\widetilde{d}_{i+1}+2} + \frac{(P_i - P_{i-1}) - Iv(\dot{X}_i + \dot{X}_{i-1})}{\widetilde{d}_i+2}\right),$$

$$\dot{P}_i = \frac{C_i}{Iv}\left(\frac{P_{i+1}-P_i}{\widetilde{d}_{i+1}+2} - \frac{P_i-P_{i-1}}{\widetilde{d}_i+2}\right) - C_i\left(\frac{\dot{X}_{i+1}-\dot{X}_i}{\widetilde{d}_{i+1}+2} - \frac{\dot{X}_i-\dot{X}_{i-1}}{\widetilde{d}_i+2}\right),$$

$$i = 1,\ldots,N-1; \tag{2.34}$$

and

$$\dot{P}_1 + 2C_1\frac{\dot{X}_2}{\widetilde{d}_1+2} = 2\frac{C_1}{Iv}\frac{P_2-P_1}{\widetilde{d}_1+2},\quad \dot{X}_1 = 0,$$
$$\dot{P}_N - 2C_N\frac{\dot{X}_2}{\widetilde{d}_{N-1}+2} = -2\frac{C_N}{Iv}\frac{P_N-P_{N-1}}{\widetilde{d}_{N-1}+2},\quad \dot{X}_N = 0. \tag{2.35}$$

Let us consider certain limiting cases for (2.34)–(2.35). In the case $\beta \to \infty$, the limiting system for the evolution of pressures and positions has the form

$$2\dot{P}_i + C_i(\dot{X}_{i+1} - \dot{X}_{i-1}) = \frac{C_i}{Iv}(P_{i+1} - 2P_i + P_{i-1}),$$
$$\dot{X}_{i+1} - 2\dot{X}_i + \dot{X}_{i-1} = \frac{P_{i+1}-P_{i-1}}{vI},\quad \text{for}\ \ i = 1,\ldots,N-1; \tag{2.36}$$

and

$$\dot{P}_1 + C_1\dot{X}_2 = \frac{C_1}{Iv}(P_2 - P_1),\quad \dot{X}_1 = 0,$$
$$\dot{P}_N - C_N\dot{X}_{N-1} = -\frac{C_N}{Iv}(P_N - P_{N-1}),\quad \dot{X}_N = 0. \tag{2.37}$$

https://doi.org/10.1017/S0956792513000314 Published online by Cambridge University Press

Next, rescaling the time by βv and proceeding to the limit $\beta \to 0$, the limiting system for the evolution of pressures and positions takes the form

$$\dot{P}_i = C_i \left(\frac{P_{i+1} - P_i}{d_{i+1}} - \frac{P_i - P_{i-1}}{d_i} \right),$$
$$\dot{X}_i = -\frac{P_i \sqrt{3\sigma} I}{2} \left(\frac{P_{i+1} - P_i}{d_{i+1}} + \frac{P_i - P_{i-1}}{d_i} \right), \quad \text{for} \quad i = 1, \ldots, N-1; \tag{2.38}$$

and

$$\dot{P}_1 = 2C_1 \frac{P_2 - P_1}{d_1}, \quad \dot{X}_1 = 0,$$
$$\dot{P}_N = -2C_N \frac{P_N - P_{N-1}}{d_N}, \quad \dot{X}_N = 0. \tag{2.39}$$

Note that the last system coincides with the one derived in [16] for the intermediate-slip equation (1.9) in the one-dimensional case. This stays in agreement with the fact that (1.9) is the limiting case of (1.5a)–(1.5b) as $\beta \to 0$ as was shown in [22, 32]. Finally, note that after time rescaling by βv and taking limits $v \to \infty$ or $v \to 0$ results again in (2.36)–(2.37) and (2.38)–(2.39), respectively. This is also natural because (1.8a)–(1.8b) and (1.9) are the limiting cases of (1.5a)–(1.5b) and $v \to \infty$ or $v \to 0$, respectively.

Let us summarize the algorithm for the simulation of coarsening dynamics in large arrays of droplets using the derived reduced ODE models. Starting with an array of $N+1$ droplets after each subsequent coarsening event (i.e collapse of one droplet or collision of two droplets) one can model the coarsening process further by reducing the dimension of the model by two and solving the reduced ODE model with the updated initial data. Practically, as in [19], we say that a collapse event occurs when pressure of one droplet increases a certain threshold, namely when

$$P > 0.5 P_{\max}(\varepsilon).$$

Note, that $P_{\max}$ introduced in (1.3) provides the pressure threshold at which droplet stationary solutions cease to exists [18, 24]. Then we take the final pressures and positions of the remaining droplets from the previous run of the reduced ODE model as initial conditions for the next one. In the case of a collision in [19] it was suggested that the coarsening event occurs when the distance between two colliding ith and $i+1$th droplets becomes smaller than a certain threshold $\delta = O(\varepsilon)$, i.e. when

$$d_i \leqslant \delta. \tag{2.40}$$

After the collision we calculate the position and pressure of a newly formed droplet by the following formulas:

$$X_{i,\text{new}} = 1/2(X_{i+1} + R_{i+1} + X_i - R_i),$$
$$P_{i,\text{new}} = \left(\frac{1}{P_i^2} + \frac{1}{P_{i+1}^2} \right)^{-1/2}, \tag{2.41}$$

i.e. the position of it is at the midpoint between the outer contact lines of old two droplets,

https://doi.org/10.1017/S0956792513000314 Published online by Cambridge University Press

while the formula for its pressure is a direct consequence of the total volume conservation and (2.33). The last formula for $P_{i,\text{new}}$ is based on the observation that the mass of the new droplet is of the leading order in ε given by the sum of the masses of the collided droplets. In Section 5.1 we compare solutions of the derived reduced ODE model (2.34)–(2.35) with those of the initial PDE system (1.5a)–(1.5b) and show that the former ones provide high accuracy $O(\varepsilon)$ also after subsequent coarsening events.

3 An exactly solvable collisions/absorption model

Let us consider the limiting case of infinite slip length $\beta = \infty$, namely the ODE system (2.36)–(2.37) describing coarsening in free films. As pressure evolution proceeds on a slower time-scale than that of one of the positions as $\varepsilon \to 0$, let us consider only the migration of droplets. Namely, we investigate the zero-order system

$$\begin{aligned} \dot{X}_0 = \dot{X}_N = \dot{P}_i = 0, \quad \text{for} \quad i = 0, \dots, N, \\ \dot{X}_{i+1} - 2\dot{X}_i + \dot{X}_{i-1} = \frac{P_{i+1} - P_{i-1}}{\nu I}, \quad \text{for} \quad i = 2, \dots, N-1. \end{aligned} \tag{3.1}$$

As will be justified numerically in Section 5.1 for given ε, $T > 0$, one can initial choose data with sufficiently small $P_i(0) \ll 1$, $i = 0, 1, \dots, N$ such that the difference between solutions to (3.1) and (2.36)–(2.37) stays uniformly $O(\varepsilon)$ for all times $t \in (0, T]$. Note that for such initial data there is no other constraint on the location of $X_i(0)$ other than that $d_i(0)$ should be larger than the collision threshold δ introduced in (2.40).

Moreover, for certain initial data one can solve (3.1) explicitly. Indeed, if

$$P_i(0) = p, \text{ for } i = 0, 1, \dots, N-1 \text{ and } P_N(0) = \bar{p} \text{ with } 1 \gg p > \bar{p}, \tag{3.2}$$

then the solution to (3.1) is given by

$$X_i(t) = X_i(0) + \frac{Bi}{N} t, \text{ for } i = 1, \dots, N-1; \; X_0 = 0, \; X_N = L, \text{ where } B = \frac{p - \bar{p}}{\nu I}. \tag{3.3}$$

Let us recall the notation for the distances between droplets

$$d_i(t) = X_i(t) - X_{i-1}(t) \text{ for } i = 1, \dots, N-1 \text{ and } d_N(t) = L - X_{N-1}(t) - R_N(t) - R_{N-1}(t),$$

where we have slightly modified it now for the last droplet, and call below $d_i(t)$ the distance of the ith droplet at time t. Using this notation one can rewrite the solution (3.3) in the following form:

$$\begin{aligned} d_i(t) = d_i(0) + \frac{B}{N} t, \quad \text{for} \quad i = 1, \dots, N-1, \\ d_N(t) = d_N(0) - \frac{B(N-1)}{N} t \text{ for } t \in (0, T_c), \text{ where } T_c = \frac{d_N(0) N}{(N-1) B}. \end{aligned} \tag{3.4}$$

Note that T_c denotes the time proceeding until the $(N-1)$th droplet collides with the largest last one. Iterating (3.4), one observes that the first $N-1$ droplets collide one after another with the last one. Due to (3.3) all droplets except the first and the last ones

https://doi.org/10.1017/S0956792513000314 Published online by Cambridge University Press

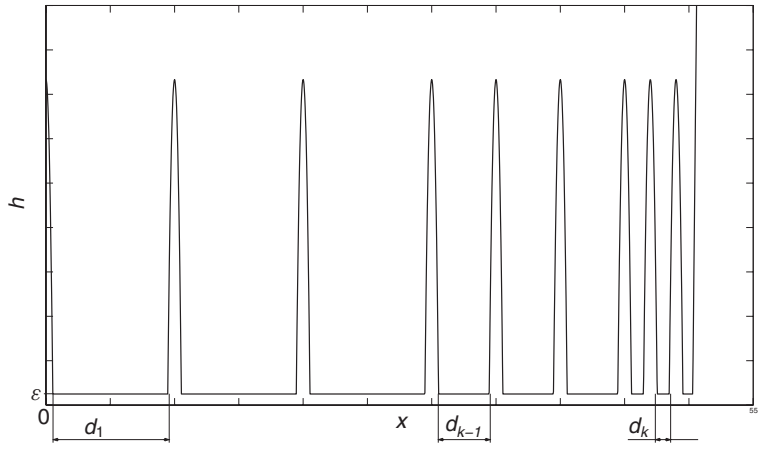

FIGURE 4. Example of an initial profile with $k = 3$ families of droplets as defined in (3.7).

move to the right. The last droplet consequently absorbs the neighbour droplet, while the distance between them is uniformly distributed between the remaining droplets. Therefore, the distances of the remaining droplets at the collision time T_c are given by

$$d_i(T_c) = d_i(0) + d_N(0)/(N-1), \quad i = 1, \ldots, N-1. \tag{3.5}$$

Writing the solution to (3.1) in the form (3.4) is convenient because one can substitute $d_i(T_c)$ as the initial distances for the modelling of the next collision event.

Note that due to (3.5) distance monotonicity is preserved in time for solutions (3.4), i.e. if $d_l(0) > d_m(0)$ for some $l, m \in 1, \ldots, N$, then $d_l(t) > d_m(t)$ for all times $t > 0$. This property allows us, based only on a given initial distribution of the distances in the array of droplets, to derive the coarsening laws analytically for solutions to (3.1) considered with (3.2) and additional assumption

$$1 \gg p \gg \bar{p}. \tag{3.6}$$

This assumption prescribes that the last droplet is much larger than others and allows us to simplify further the dynamics by assuming that its pressure $P_N(t)$ remains to be the leading order constant in time and equal to $\bar{p}$. In turn, this implies that the coarsening dynamics in this case depends solely on the evolution of droplet positions without change of their pressures after subsequent collisions.

Indeed, for a given set of initial distances, let us divide it into $k \leqslant N$ families (subsets) such that there are i_m distances in mth family ($1 \leqslant m \leqslant k$), all of them are equal to d_m and

$$d_1 \geqslant d_2 \geqslant \ldots \geqslant d_k, \quad i_1 + i_2 + \cdots + i_k = N \tag{3.7}$$

holds. In addition, let us allocate these k families in the initial configuration so that the distances between droplets non-increase coming from the first to the last droplet (see Figure 4). Then due to the distance monotonicity property, this ordering will be preserved in time, i.e. first the members of the family k will be absorbed by the last droplet, then those of $(k-1)$th family etc. Moreover, distances in each family will stay equal for all

https://doi.org/10.1017/S0956792513000314 Published online by Cambridge University Press

$t > 0$. This implies that for the initial data satisfying (3.2), (3.6) and (3.7) all collision times are uniquely determined having given k and the set $\{d_m, i_m\}$, $m = 1, \dots, k$. Therefore, using the explicit solution (3.4) holding between subsequent collision events, the corresponding coarsening law can be derived analytically by a recursive procedure.

Indeed, let us fix an index $1 \leqslant m \leqslant k$ and look at the moment when all families with the indexes $m+1, \dots, k$ and also $l-1$ members of the mth family have been absorbed for some given $1 \leqslant l \leqslant i_m$. Let us calculate time $t(n)$ needed for the absorption of the lth member with n denoting the remaining number of droplets after the latter event. Using (3.4), one can easily calculate by recursion that

$$t(n) = \frac{n+1}{nB}\left(\widetilde{d}_m + \sum_{r=1}^{l-1} \frac{t(n+r)B}{n+r+1}\right) = \frac{(n+l)\widetilde{d}_m}{nB}, \tag{3.8}$$

where by $\widetilde{d}_m$ we denote the distance in the mth family at the time when $(m+1)$th family has been absorbed. From (3.8) one can obtain the total time needed for the mth family to be absorbed, T_m, in the form

$$T_m = \frac{\widetilde{d}_m}{B}\left(N - \sum_{p=m+1}^{k} i_p\right) \sum_{r=1}^{i_p} \frac{1}{N - \sum_{p=m+1}^{k} i_p - r}. \tag{3.9}$$

In turn, using again (3.4), one recursively finds

$$\widetilde{d}_m = \sum_{p=m+1}^{k} \frac{\widetilde{d}_p i_p}{N - \sum_{p'=p}^{k} i_p} = \frac{\sum_{p=m+1}^{k} d_p i_p}{N - \sum_{p'=p}^{k} i_p} + d_m.$$

Substituting the last expression in (3.9) one obtains

$$T_m = \frac{1}{B}\left(N d_m + \sum_{p=m}^{k} (d_p - d_m) i_p\right) \sum_{r=1}^{i_m} \frac{1}{N - \sum_{p=m+1}^{k} i_p - r}.$$

Therefore, the total time needed for all families up to mth to be absorbed is given by

$$T(d_m) = \sum_{p=m}^{k} \frac{1}{B}\left(N d_p + \sum_{p'=p}^{k} (d'_p - d_p) i'_p\right) \sum_{r=1}^{i_p} \frac{1}{N - \sum_{p'=p+1}^{k} i'_p - r}. \tag{3.10}$$

Let us now derive the continuum version for the discrete coarsening law in (3.10), proceeding to the limits $N \to \infty$ and $k \to \infty$. Suppose we are given a probability density function $f(d)$ on $(0, +\infty)$, i.e.

$$\int_0^{+\infty} f(x)\, dx = 1, \quad f(d) \geqslant 0 \text{ and } f(d) = 0 \text{ if } d \leqslant 0.$$

Defining $d_i = i\Delta d$ for $i \in \mathbb{N} \cup \{0\}$ and a fixed $\Delta d \ll 1$, we approximate $f(d)$ by a piece-wise constant function $f_a(d)$ as follows:

$$f_a(d) = f(d_{i+1}) \text{ for } d \in [d_i, d_{i+1}) \text{ and } f_a(d) = 0 \text{ if } d \leqslant 0.$$

https://doi.org/10.1017/S0956792513000314 Published online by Cambridge University Press

Accordingly to this approximation, suppose we are given an array of $N+1$ droplets with $N \gg 1$ such that the number of droplets with the distances lying in the interval $[d_i, d_{i+1})$ is equal to $[Nf(d_{i+1})\Delta d]$. As before, we suppose that droplets are allocated so that the distances between them are non-increasing and (3.2) and (3.6) hold. Then using (3.10) one obtains

$$\begin{aligned} T_{\Delta d,N}(d_m) &= \sum_{p=0}^{m} \frac{1}{B} \left(N d_p + \sum_{p'=p}^{k} (d'_p - d_p) N f(d'_p) \Delta d \right) \\ &\quad \sum_{r=1}^{Nf(d_p)\Delta d} \frac{1}{N - \sum_{p'=p+1}^{k} N f(d'_p)\Delta d - r} + O(\Delta d, 1/N) \\ &= \sum_{p=0}^{m} \frac{1}{B} \left(d_p + \sum_{p'=p}^{k} (d'_p - d_p) f(d'_p) \Delta d \right) \\ &\quad \sum_{r=1}^{Nf(d_p)\Delta d} \frac{1}{1 - \sum_{p'=p+1}^{k} f(d'_p)\Delta d - r/N} + O(\Delta d, 1/N) \\ &= \sum_{p=0}^{m} \frac{N}{B} \left(d_p + \sum_{p'=p}^{k} (d'_p - d_p) f(d'_p) \Delta d \right) \\ &\quad \sum_{s=1/N}^{f(d_p)\Delta d} \frac{\Delta s}{1 - \sum_{p'=p+1}^{k} f(d'_p)\Delta d - s} + O(\Delta d, 1/N). \end{aligned}$$

Taking the limit $N \to +\infty$ in the last expression and introducing

$$T_{\Delta d}(d) = \lim_{N \to +\infty} \frac{T(d)_{\Delta d,N}}{N},$$

one obtains

$$T_{\Delta d}(d) = \sum_{p=0}^{m} \frac{N}{B} \left(d_p + \sum_{p'=p}^{k} (d'_p - d_p) f(d'_p) \Delta d \right) \int_{s=0}^{f(d_p)\Delta d} \frac{ds}{1 - \sum_{p'=p+1}^{k} f(d'_p)\Delta d - s} + O(\Delta d). \tag{3.11}$$

Applying the Taylor expansion to the last integral in (3.11), one finds

$$\int_{s=0}^{f(d_p)\Delta d} \frac{ds}{1 - \sum_{p'=p+1}^{k} f(d'_p)\Delta d - s} = \frac{f(d_p)\Delta d}{1 - \sum_{p'=p}^{k} f(d'_p)\Delta d} + O(\Delta d^2).$$

Inserting this into (3.11), one obtains

$$T_{\Delta d}(d) = \frac{1}{B} \sum_{p=0}^{m} \left(d_p + \sum_{p'=p}^{k} (d'_p - d_p) f(d'_p) \Delta d \right) \frac{f(d_p)\Delta d}{1 - \sum_{p'=p}^{k} f(d'_p)\Delta d} + O(\Delta d).$$

https://doi.org/10.1017/S0956792513000314 Published online by Cambridge University Press

Finally, taking the limit $\Delta d \to 0$ and introducing

$$T(d) = \lim_{\Delta d \to 0} \frac{T_{\Delta d}(d)}{N},$$

one arrives at

$$T(d) = \frac{1}{B} \int_0^d \left(x + \int_0^x (y - x) f(y)\, dy \right) \frac{f(x)}{1 - \int_0^x f(y)\, dy}\, dx. \tag{3.12}$$

Introducing function $n(d)$ as the relative number of droplets with initial distances larger or equal to d, i.e. as

$$n(d) = 1 - \int_0^d f(x)\, dx, \tag{3.13}$$

one obtains from (3.12) that

$$\begin{aligned} T(d) &= \frac{1}{B} \int_0^d \left(-x + \int_0^x (y - x) n'(y)\, dy \right) \frac{n'(x)}{1 - \int_0^x n(y)\, dy}\, dx \\ &= \frac{1}{B} \int_0^d n(x) \ln \left[\frac{n(x)}{n(d)} \right] dx. \end{aligned} \tag{3.14}$$

The last expression provides an exact coarsening law, i.e. it tells what time $T(d)$ will pass until all droplets having initially distances smaller then d are absorbed by the last large droplet.

In Appendix B, we show that the discrete coarsening law (3.10) can be recovered back from (3.14) if the initial distribution $f(x)$ has the form

$$f(d) = \sum_{m=1}^{k} i'_m \delta(d - d_m), \tag{3.15}$$

i.e. it is represented by $k \in \mathbb{N}$ families as in (3.7), while the number of droplets $N \to \infty$. Moreover, in Section 5.2 we justify numerically the connection between (3.14), (3.10) and the starting ODE system (3.1).

4 Examples of coarsening rates

Example 1. We consider an explicit family of initial distributions $f(x)$ and show that depending on their decay as $x \to +\infty$ the coarsening rates reproduce all possible algebraic decays. Moreover, there is a certain threshold after which the decay becomes exponential. Namely, let us consider

$$f(x) = \frac{1}{x^{1+\alpha}} \Big/ \int_A^{+\infty} \frac{dx}{x^{1+\alpha}} = \frac{A^\alpha}{x^{1+\alpha}} \quad \text{with} \quad \alpha, A > 0. \tag{4.1}$$

From (3.13) it follows that

$$n(x) = \left(\frac{A}{x} \right)^\alpha. \tag{4.2}$$

https://doi.org/10.1017/S0956792513000314 Published online by Cambridge University Press

Substituting this in (3.14) one obtains

$$T(d) = \frac{\alpha A}{B(\alpha-1)}\left(\frac{1}{\alpha-1}\left[\left(\frac{d}{A}\right)^{1-\alpha}-1\right]+\alpha\ln\left[\frac{d}{A}\right]\right) \text{ if } \alpha \neq 1, \tag{4.3a}$$

$$T(d) = \frac{A}{B}\left(\left[\ln\left(\frac{d}{A}\right)\right]^2/2+\ln\left(\frac{d}{A}\right)\right) \text{ if } \alpha = 1. \tag{4.3b}$$

Combining (4.3b) and (4.2) one obtains the exact coarsening law for the case $\alpha = 1$,

$$n(t) = \exp\left[1-\sqrt{1+2Bt/A}\right]. \tag{4.4}$$

In the case $\alpha \neq 1$ one obtains from (4.3a) and (4.2)

$$T(n) = \frac{\alpha A}{B(\alpha-1)}\left(\frac{1}{1-\alpha}\left[n^{\frac{\alpha-1}{\alpha}}-1\right]+\ln(n)\right).$$

For the latter exact law one obtains the following asymptotics

$$n(t) \sim \begin{cases} \left(\dfrac{tB(\alpha-1)^2}{\alpha A}\right)^{\frac{\alpha}{\alpha-1}}, & \text{if } \alpha < 1 \\ \exp\left\{-\dfrac{tB(\alpha-1)}{\alpha A}\right\}, & \text{if } \alpha > 1 \end{cases} \quad \text{as } t \to \infty. \tag{4.5}$$

Therefore, from (4.4)–(4.5) one finds out that for $0 < \alpha < 1$ the coarsening rates are algebraic at least for large times, while at $\alpha = 1$ they become exponential and stay so for $\alpha \in (1, +\infty)$.

Example 2. Consider $f(x) = \exp(-x)$. Substituting it in (3.13) and (3.14), consequently, one obtains the exact law

$$T(n) = \frac{1}{B}(n-1-\ln(n)).$$

Thus, in this case the following asymptotics holds

$$n(t) \sim \exp(-Bt) \quad \text{as} \quad t \to \infty. \tag{4.6}$$

Example 3. Consider a Gaussian distribution $f(x) = 2/\sqrt{\pi}\exp(-x^2)$. In this case by (3.13) one has $n(x) = \operatorname{erfc}(x)$. Substituting it in (3.14) one obtains

$$\begin{aligned} T(d) &= \frac{1}{B}\int_0^d\left[\int_0^x n(y)\,dy\right]\frac{n'(x)}{n(x)}\,dx \\ &= \frac{1}{B\sqrt{\pi}}\int_0^d\left(\frac{(1-\exp(-x^2))\exp(-x^2)}{\int_x^{+\infty}\exp(-x^2)\,dt}-2x\exp(-x^2)\right)dx \\ &= \frac{1}{B\sqrt{\pi}}\left(-C+O\left(\exp(-d^2)\right)+\int_0^d\frac{\exp(-x^2)}{\int_x^{+\infty}\exp(-x^2)\,dt}\,dx\right) \\ &= \frac{1}{B\sqrt{\pi}}(-C-\ln(n(d)))+O(\exp(-d^2)), \end{aligned}$$

https://doi.org/10.1017/S0956792513000314 Published online by Cambridge University Press

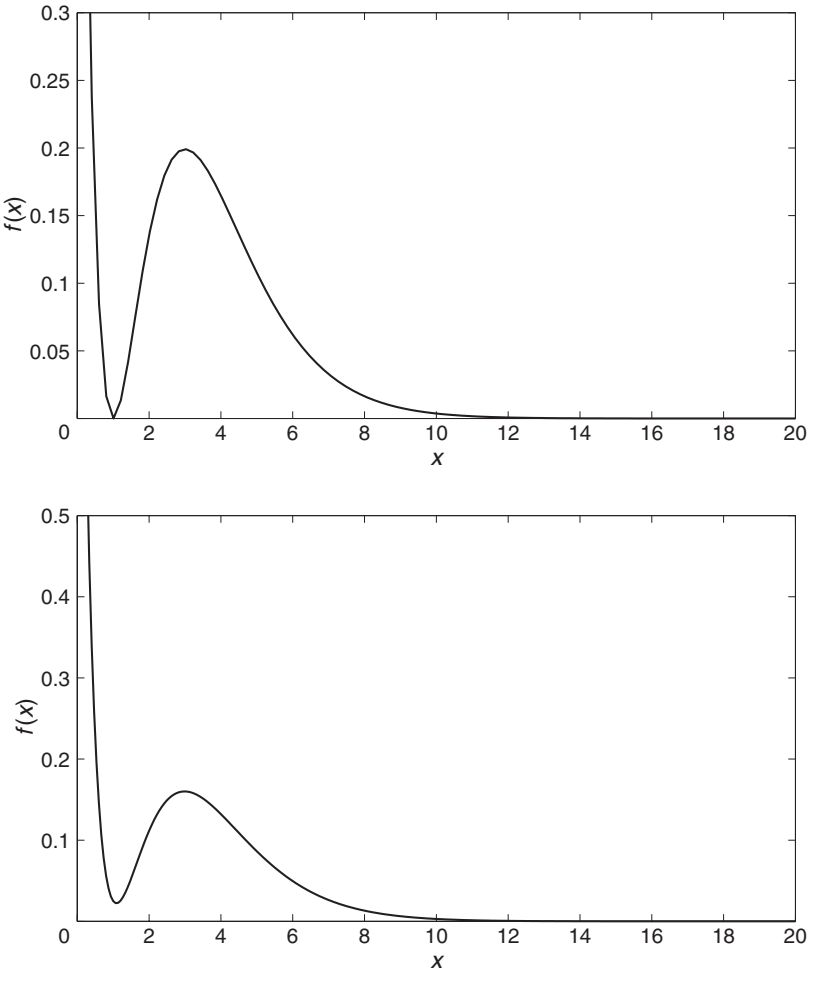

FIGURE 5. Initial distributions in Example 4 (left), and Example 5 with $\alpha = 2$ (right).

where constant $C \approx 0.74$. Therefore, the following asymptotics holds:

$$n(t) \sim \exp\{-C - B\sqrt{\pi}t\} \quad \text{as} \quad t \to \infty, \tag{4.7}$$

and the coarsening rates show an exponential decay as in the example 2.

Example 4. Finally, let us show that the coarsening rates for large times depend only on how fast the initial distribution $f(x)$ decays as $x \to +\infty$ and not on its behaviour for moderate x. In this and the next example we consider non-monotone distributions having a local maximum at $x > 0$. Consider $f(x) = (1 - x)^2 \exp(-x)$ (see Figure 5) with

https://doi.org/10.1017/S0956792513000314 Published online by Cambridge University Press

$n(x) = (1 + x^2)\exp(-x)$ correspondingly. By (3.14) one obtains

$$\begin{aligned} BT(d) &= \int_0^d (1+x^2)\exp(-x)\ln(1+x^2)\,dx - \int_0^d x(1+x^2)\exp(-x)\,dx \\ &\quad - (\ln(1+d^2) - d)\int_0^d (1+x^2)\exp(-x)\,dx \\ &= \int_0^d (1+x^2)\exp(-x)\ln(1+x^2)\,dx - 7 + 3(d - \ln(1+d^2)) + O(\exp(-d)). \end{aligned} \tag{4.8}$$

The first integral in the last expression can be estimated as follows:

$$\begin{aligned} \int_0^d (1+x^2)\exp(-x)\ln(1+x^2)\,dx &\leqslant \ln(1+d^2)\int_0^d (1+x^2)\exp(-x)\,dx \\ &= \ln(1+d^2)(3 + O(\exp -d)). \end{aligned}$$

Combining this with (4.8) one obtains

$$T(d) = \frac{3d}{B} + o(d),$$

and hence the following asymptotics holds:

$$n(t) \sim \left(1 + \frac{9}{B^2}t^2\right)\exp(-Bt) \quad \text{as} \quad t \to \infty.$$

Therefore, the coarsening rates show an exponential decay as in Example 2.

Example 5. Consider distributions

$$\frac{\alpha}{\alpha+1}\left[(1-x)^2\exp(-x) + 1/(1+x)^{1+\alpha}\right] \quad \text{with} \quad \alpha > 0,\ \alpha \neq 1. \tag{4.9}$$

These have a local maximum at $x > 0$ and a decay $\sim 1/x^{1+\alpha}$ as $x \to \infty$ (see Figure 5). Correspondingly, one has

$$n(x) = \frac{1}{1+\alpha}\left[(1+x)^{-\alpha} + \alpha\exp -x(1+x^2)\right].$$

Substituting it in (3.14) one obtains

$$\begin{aligned} BT(d) &= \int_0^d \left[\int_0^x n(y)\,dy\right]\frac{n'(x)}{n(x)}\,dx \\ &= \int_0^d \left[\frac{1}{1-\alpha}\left((1+x)^{1-\alpha} - 1\right) + \alpha\left(3 - \exp(-d)(3 + d(2+d))\right)\right] \\ &\quad \times \frac{(1-x)^2\exp(-x) + (1+x)^{-1-\alpha}}{(1+x)^{-\alpha} + \alpha\exp(-x)(1+x^2)}\,dx. \end{aligned}$$

The last integral can be bounded from below and above by integrals of the following type

$$I^* = \int_0^d \left[\frac{1}{1-\alpha}\left((1+x)^{1-\alpha} - 1\right) + C_1\right]\frac{C_2\exp(-x/2) + (1+x)^{-1}}{1 + C_3}$$

https://doi.org/10.1017/S0956792513000314 Published online by Cambridge University Press

with some non-negative constants C_i, $i = 1, 2, 3$. Integrals in (4) have the following asymptotics:

$$I^* = C_3 \left(\frac{1}{1-\alpha} \left[(d+1)^{1-\alpha} - 1 \right] - C_4 \ln(d+1) \right) + O(1) \quad \text{as} \quad d \to \infty$$

with some positive constants C_3, C_4. Therefore, using

$$n(d) \sim \frac{1}{1+\alpha} (1+d)^{-\alpha} \quad \text{as} \quad d \to \infty \tag{4.10}$$

one obtains that the asymptotics of the coarsening law for (4.9) coincides up to multiplicative constants with (4.3a) already obtained in Example 1 for monotone distributions. Consequently, we conclude that as in Example 1 the coarsening rates are algebraic with power $\alpha/(\alpha-1)$ for $\alpha < 1$ and exponential for $\alpha > 1$.

A more simple but rather formal proof of this fact is as follows. Let us fix a large number A such that asymptotics (4.10) holds for all $d > A$ with a good precision. Then one has

$$\begin{aligned} BT(d) &= \int_0^A n(x) \ln \left[\frac{n(x)}{n(d)} \right] dx + \int_A^d n(x) \ln \left[\frac{n(x)}{n(d)} \right] dx \\ &\sim O(1) + \alpha \ln(d+1) \times O(1) + \int_A^d n(x) \ln \left[\frac{n(x)}{n(d)} \right] dx. \end{aligned}$$

The last integral in view of (4.10) is of the type considered already in Example 1. Therefore, the term $O(1) + \alpha \ln(d+1) \times O(1)$ produces no change in the asymptotics of $T(d)$, and consequently the coarsening law coincides up to multiplicative constants with (4.3a).

5 Numerics

In the last two sections starting from system (1.5a)–(1.5b) we first derived a closed ODE model (2.34)–(2.35) describing coarsening dynamics in an array of initial $N+1$ metastable droplets. Then we looked at its limiting case $\beta \to \infty$ described by (2.36)–(2.37) and more precisely on its zero-order version as $\varepsilon \to 0$ given by (3.1). Next, we found out that for a special initial data satisfying (3.2) one can obtain the explicit solution to (3.1) given by (3.4). Assuming additionally (3.6) and that the distances in the array are ordered non-increasingly, we derived the explicit coarsening law (3.10). Finally, we obtained its continuous counterpart (3.14). In this section we systematically compare numerically the solutions of subsequent models in the derived model hierarchy and check coarsening laws (3.10) and (3.14).

5.1 Comparison between models

Here we compare solutions to the full ODE system (2.34)–(2.35) with those of the strong-slip system (1.5a)–(1.5b) and its limiting cases (1.9) and (1.8a)–(1.8b) as $\beta \to 0$ and $\beta \to +\infty$, respectively. For the solution of PDE systems we used a fully implicit finite difference

https://doi.org/10.1017/S0956792513000314 Published online by Cambridge University Press

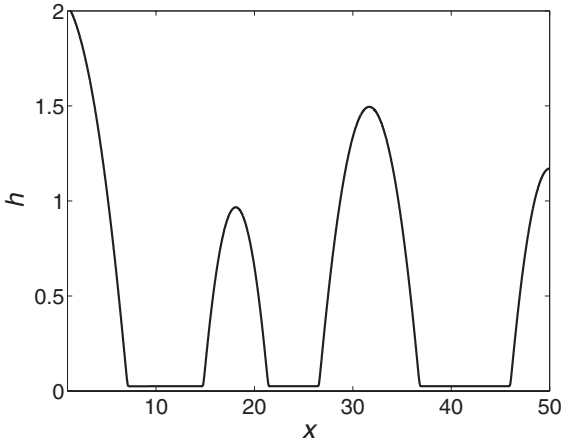

FIGURE 6. Initial profile of four droplets used for numerical simulations in Figures 7 and 8.

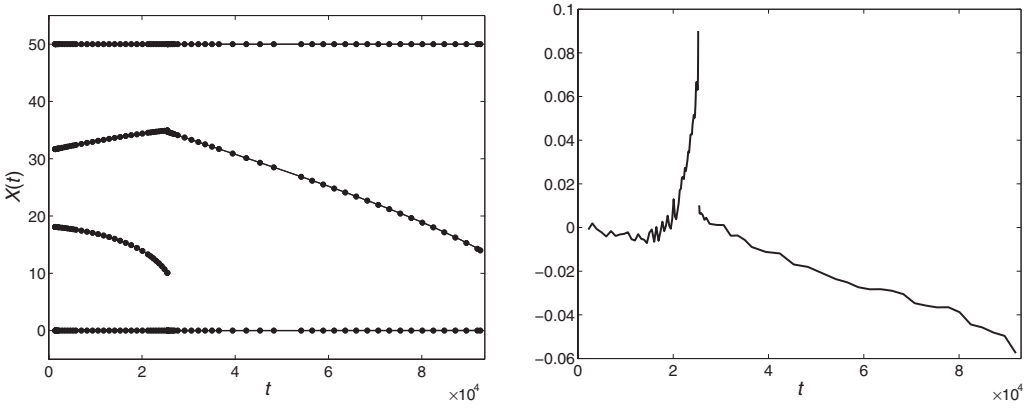

FIGURE 7. Comparison of droplet position evolution obtained from the ODE model (dots) and the lubrication model (solid line) in the strong-slip case with $\varepsilon = 0.025$, $Re = 1$, $\sigma = 1$, $\nu = 4$ and $\beta = 10$. Initial profile of four droplets shown in Figure 6 was used. Left plot: Subsequent collisions of the second and the third droplets with the first one are shown. Right plot: The corresponding deviations between the results of the ODE model and the lubrication model for the positions of the second and the third droplets, respectively, are shown.

scheme derived and applied already to (1.5a)–(1.5b) and its limiting cases in [21,30,32,35]. The numerical solutions for (2.34)–(2.35) were obtained applying the fourth-order adaptive time-step Runge–Kutta method and using updating rules (1.3)–(2.41) after each subsequent coarsening event. In the case of the PDE system, the corresponding pressure evolution was calculated using finite-difference discretization of the term $\Pi_\varepsilon(h) - \partial_{xx}h$.

In Figure 7 starting from an array of four droplets we compare evolution of positions resulting from PDE and ODE models for two subsequent collisions. Figure 7 shows that the absolute deviation between results stays uniformly $O(\varepsilon)$ also after subsequent collision events.

https://doi.org/10.1017/S0956792513000314 Published online by Cambridge University Press

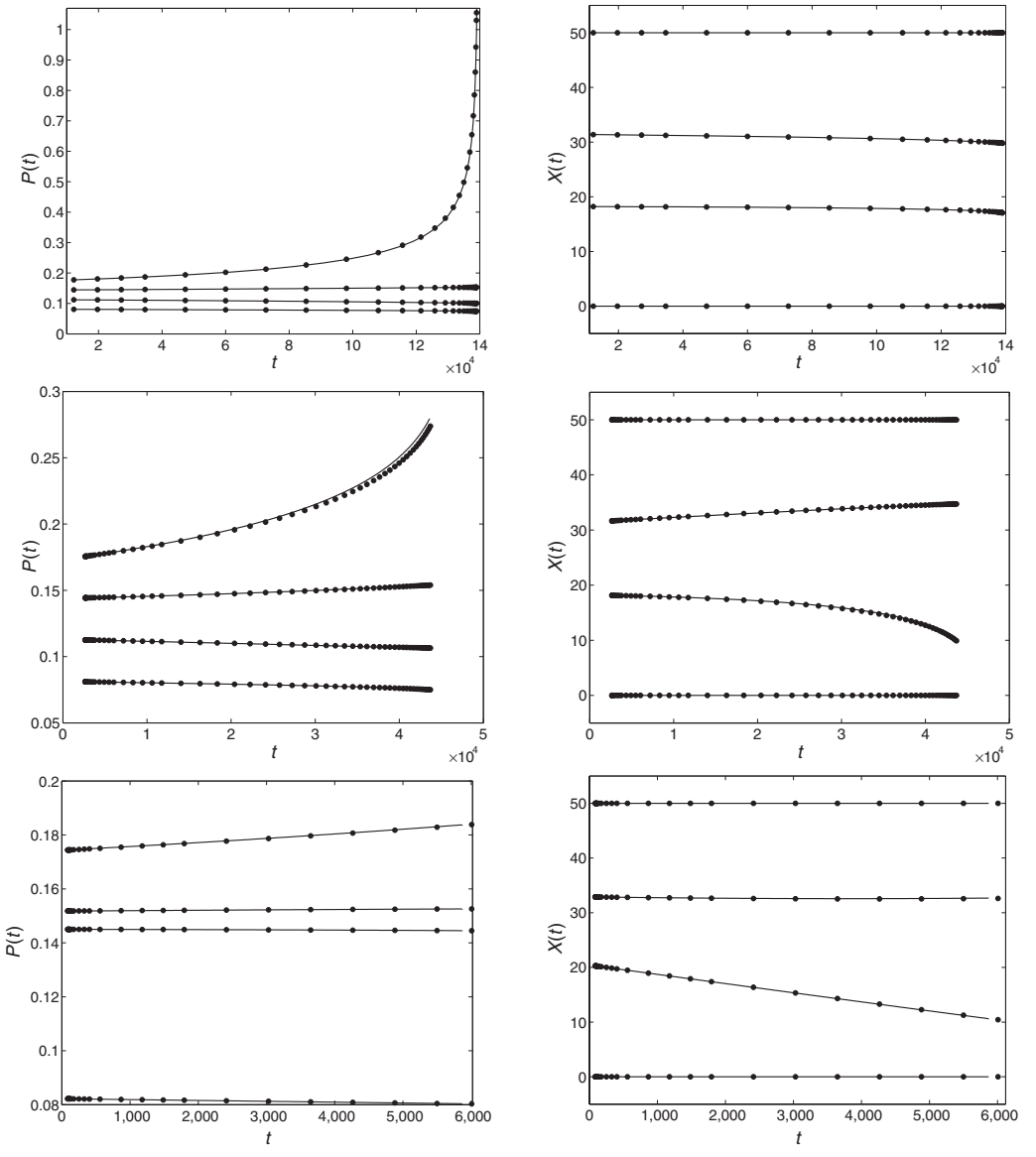

FIGURE 8. Comparison of droplet evolution obtained from the ODE model (dots) and the lubrication model (solid line) in the strong-slip case with $\varepsilon = 0.025$, $Re = 1$, $\sigma = 1$, $\nu = 4$ and different β. Initial profile of four droplets shown in Figure 6 was used. Upper row: Pressure and position evolution in the intermediate-slip case ($\beta = 0$) until collapse of the second droplet. Starting from the same initial profile, pressure and position evolution until the collision of the second droplet with the first one for $\beta = 5$ (second row) and $\beta = \infty$ (bottom row) are shown.

In Figure 8 starting from the same array of four droplets we compare solutions for different slip lengths β. In the cases $\beta = 0$ and $\beta = \infty$ we compared solutions to (1.9) and (1.8a)–(1.8b) with those of (2.38)–(2.39) and (2.36)–(2.37), respectively. Again for all β the absolute deviation between PDE and ODE results is $O(\varepsilon)$. Figure 8 demonstrates the fact

https://doi.org/10.1017/S0956792513000314 Published online by Cambridge University Press

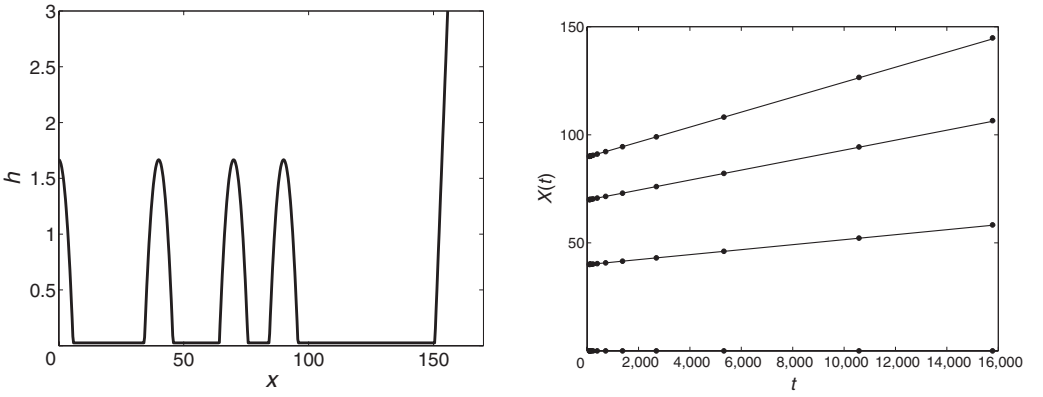

FIGURE 9. Comparison of droplet position evolution obtained from the ODE model (2.36)–(2.37) (dots) with $\varepsilon = 0.025$, $\sigma = 1$, $\nu = 4$ and its zero-order subsystem (3.1) (solid line). Left plot: The initial profile of five droplets. Pressures of the first four and the last droplets are 0.01 and 0.001, respectively. Right plot: Collision of the fourth droplet with the largest last one.

already pointed in [17, 24] that in the intermediate-slip case the coarsening dynamics is mostly governed by collapse mechanism, while in the strong-slip case with moderate and large β it is governed by collisions.

Finally, Figure 9 shows that for arrays being taken initially with sufficiently small pressures, the migration subsystem (3.1) approximates with high accuracy (at least $O(\varepsilon)$) the full ODE system (2.36)–(2.37) describing the case $\beta = \infty$. Note that the migration path of the fourth droplet in Figure 9 is considerably large, $\approx$50. Hence, the reduction from (2.36)–(2.37) to (3.1) does not constrain the initial distances to be small.

5.2 Coarsening rates

Here using the explicit solution (3.4) for the system (3.1) we check numerically the discrete and continuous coarsening laws (3.10) and (3.14). In Figure 10 we take $k = 20$ families of initial distances as prescribed in (3.7) with the corresponding pressures satisfying (3.2) and (3.6) and order them non-increasingly in space. Next, we compare the subsequent times for each mth family ($1 \leqslant m \leqslant k$) to be absorbed given, on the one hand, by the analytical law (3.10), and on the other, by the iterative calculation using (3.4) and (3.5) between subsequent collisions. Naturally, one finds out the exact coincidence between them. As each collision comprises an absorption by the largest droplet of a smaller, one does not need to update the position and pressure of the former one. This is because its position is fixed due to (2.32) to $x = L$, and the pressure to the leading order does not change due to (3.6).

In Figure 11 we show numerical results for continuous coarsening rates for three initial distributions taken from the family (4.1) with different α and one Gaussian distribution considered in Examples 1 and 3 of Section 4, respectively. To obtain the coarsening rates numerically we first sampled $N \gg 1$ distances according to the given initial distribution. After ordering them non-increasingly in the initial configuration we substitute them as initial data into (3.1) and solve the latter one iteratively using (3.4)–(3.5). Note that due

https://doi.org/10.1017/S0956792513000314 Published online by Cambridge University Press

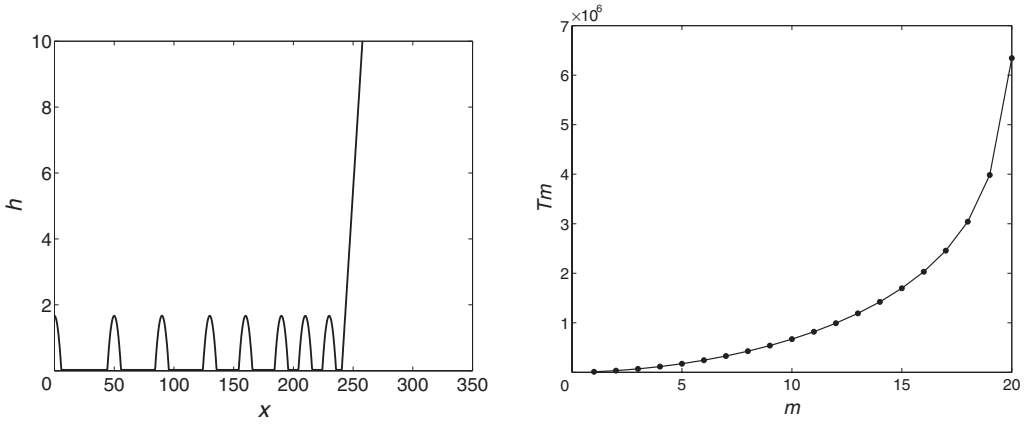

FIGURE 10. Comparison of subsequent collision/absorption times for each mth family ($1 \leqslant m \leqslant 20$) given by the discrete coarsening law (3.10) (dots) and iterative calculation using the solution (3.4) (solid line). Left plot: a part of a typical initial profile under consideration. Right plot: plot of the absorption times versus the family number.

to an extremal simplicity of (3.5) one can effectively model numerically a huge number of droplets $N \approx 10^7$ just using capabilities of a personal computer.

Figure 11 shows that thus obtained numerical coarsening rates coincide for large times very well with the analytical ones prescribed by law (3.14) and found out in Examples 1 and 3 of Section 4. In the case of (4.1) with $\alpha = 1$ one has the exact coarsening law (4.4) and therefore a good coincidence for all times. In the case of (4.1) with $\alpha \neq 1$ we compared our numerical results with the asymptotic law (4.5), and for the Gaussian initial distribution we compared with (4.7). Note that a certain deviation between numerics and analytical laws starting at the very end of the considered time interval is caused by a numerical error increase in sampling of large distances according to initial probability distributions.

6 Conclusions and discussion

In this paper we started from the high-order lubrication system (1.5a)–(1.5b) describing dewetting process in nanometric polymer film interacting on a hydrophobically coated solid substrate in the presence of large slippage at the liquid/solid interface. This system describes a distinguished and important regime within a lubrication scaling. In particular, it incorporates as a limiting case of infinite slip length the well-known model of free films (1.8a)–(1.8b) studied intensively in applications [13, 20]. Note that a system similar to (1.8a)–(1.8b) system appears in the study of viscoelastic threads for which coarsening dynamics of interacting droplets was also observed in the experiments, see e.g. [9].

Motivated by this we derived the reduced ODE models (2.34)–(2.39) describing coarsening dynamics of droplets governed by (1.5a)–(1.5b) and its limiting cases. In the limiting case $\beta = \infty$ we observed that the migration subsystem (3.1) can be solved explicitly for special initial data satisfying (3.2) and (3.6). By (3.4)–(3.5) the dynamics of droplets

https://doi.org/10.1017/S0956792513000314 Published online by Cambridge University Press

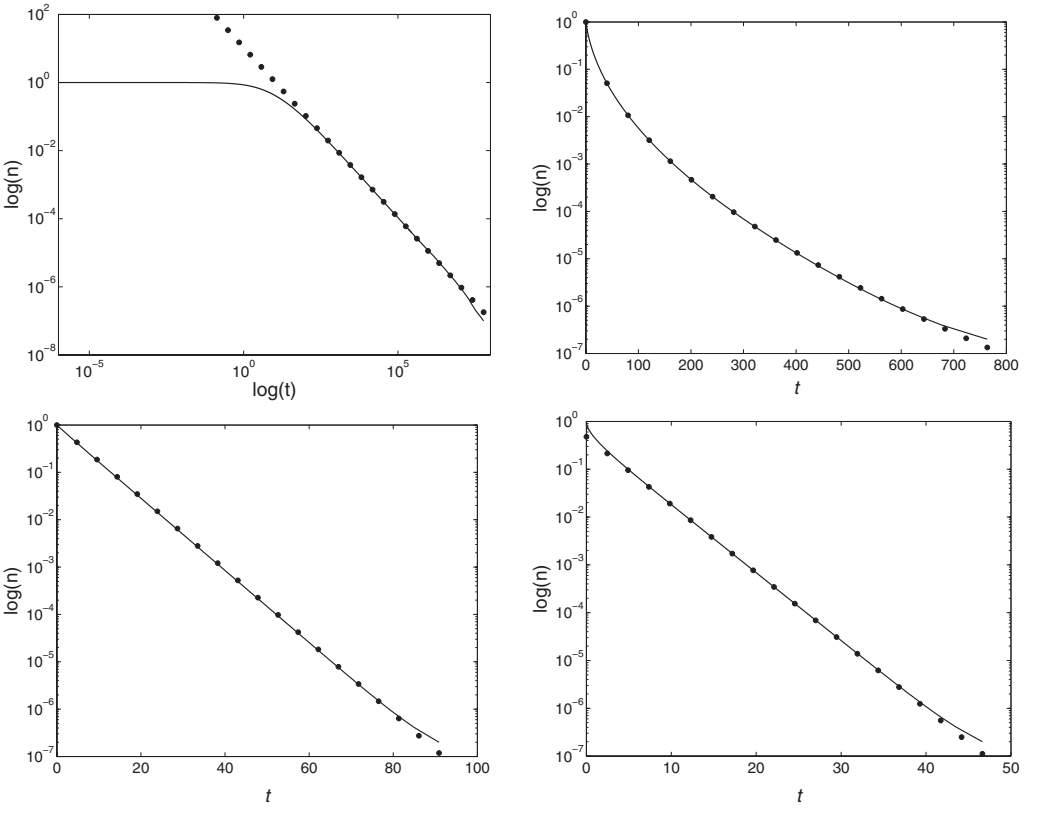

FIGURE 11. Comparison of numerical coarsening rates using sampling of initial data with $N \gg 1$ and subsequent iterative calculation using (3.4)–(3.5) (solid line) with those provided by the analytical law (3.14) (dots). Upper row: log-log and semi-log plots for the initial distribution (4.1) with $\alpha = 1/2$ (left) and $\alpha = 1$ (right), respectively. Lower row: semi-log plots for (4.1) with $\alpha = 20$ (left) and for the Gaussian initial distribution (right). According to (4.5) and (4.7) in the chosen axis scales the dots reproduce linear functions except for the upper-right plot where they represent law (4.4)

consists of sequential collisions of smaller ones with the largest one, while the distance between them is distributed uniformly between the remaining drops.

Similar models were suggested for collapse/collision dynamics of breath figures by Derrida *et al.* [12] based on heuristic arguments. There authors considered the 'cut-in-two' and 'past-all' models where the distance of the smallest droplet was divided between two neighbours or pasted as a whole to one of them. Later the breath figures of [12] found interesting analogs in the reduced coarsening models arising from the Allen–Cahn and Ginzburg–Landau equations, see e.g. a review paper [5]. A recent generalization of these models and rigorous analysis of their self-similar solutions can be found in [27]. Note that (3.1) can be classified due to (3.5) as a 'cut uniformly between all' type model. We are not aware if any heuristic or rigorous analog of it was considered so far in the literature.

Remarkably, our model (3.1) appears as a reduction of a complicated dynamics governed by a high-order lubrication system (1.8a)–(1.8b). Moreover, in contrast to the

https://doi.org/10.1017/S0956792513000314 Published online by Cambridge University Press

stochastic models of [12] if the initial distances in (3.1) are ordered non-increasingly, then they coarsen in a deterministic and exactly solvable scenario. For the latter case we derived the coarsening laws (3.10) and (3.14) analytically and confirmed them numerically. Interestingly, the derived law (3.14) has a form similar to Shannon's entropy with respect to a certain normalization of the droplet number function $n(x)$. The explanation of this fact from the statistical point of view will be presented elsewhere.

Surprisingly, in contrast to the coarsening dynamics governed by reduced ODE models arising from (1.1) which always obey law (1.12), our simple model (3.1) can reproduce any algebraic coarsening rates between zero and infinity as well as exponential ones. Moreover, for a family of initial distributions (4.1) we showed existence of a threshold for their decay at infinity at which the corresponding coarsening rates switch from algebraic to exponential ones. Note that a similar situation was accounted recently for self-similar solutions to the Smoluchowski coagulation equation with certain kernels, see [28, 29].

In view of above observations it would be natural to extend our deterministic collision/absorption model to its stochastic variant withdrawing the non-increasing initial ordering of distances and thus allowing collisions of random droplets with the largest one. As in [12], one could probably look for self-similar solutions of mean-field approximations for thus arising stochastic collision models. A further generalization of the model could be a withdrawal of constraints on the initial data (3.2), (3.6) and thus allowing droplets to collide and collapse inside of the domain. Note that then an additional difficulty to handle the pressure and position update according to coarsening rules (1.3)–(2.41) would appear. It would also be interesting to analyse the coarsening rates of full ODE model (2.34)–(2.35) considered with moderate slip-lengths $0 < \beta < \infty$. Also, the limiting case of very large Reynolds numbers which violate balance in (2.4) may imply new interesting effects on coarsening dynamics and slopes (see [21, chapter 2]), although physical validity of such regime should be justified first.

Finally, it could be possible to derive two-dimensional analogs of reduced ODE models (2.34)–(2.39) describing physically coarsening of three-dimensional droplets on a plane substrate. The two-dimensional reduced ODE models arising from (1.1) were derived in [16, 17]. In [16] a mean-filed approximation for the fluxes between droplets was suggested under an assumption of well separation of droplets that is unfortunately not suitable for the modelling of droplet collisions because the distance between them then tends to zero. In this case one should face a problem of solving a Laplace equation (counterpart to equation (2.12) in two dimensions) in a complex domain between droplets occupied by the PL region. We expect the same problem to appear for the two-dimensional reduced ODE models corresponding to (1.5a)–(1.5b).

Acknowledgements

The author acknowledges the post-doctoral scholarship at the Max-Planck Institute for Mathematics in the Natural Sciences, Leipzig and thanks Gennady Chuev, Christian Seis, Andre Schlichting and Barbara Wagner for fruitful discussion.

Appendix A Integral *I*

Here we show that integral I defined in (2.17) converges and integrates explicitly. Changing variable in (2.17) according to the explicit solution (2.6a) in the CL region, and using matching conditions (2.5) one obtains

$$I = \int_{-\infty}^{+\infty} \frac{1}{H_1}\partial_z\left(\frac{\partial_z H_1}{H_1}\right) dz = \int_1^{+\infty} \left[\frac{U'(H)}{H^2} - \frac{2(U(H)-U(1))}{H^3}\right] \frac{dH}{\sqrt{2(U(H)-U(1))}}$$

$$= \int_1^{+\infty} \frac{-5/3 + 2H - 1/3H^3}{\sqrt{2/3 - H + H^3/3}\, H^{9/2}}\, dH.$$

Let us make a further change of variables $t = 1/H$ and integrate I explicitly as follows.

$$I = \int_0^1 \frac{-5/3t^4 + 2t^3 - 1/3}{\sqrt{2/3t^3 - t^2 + 1/3}}\, dt = \int_0^1 \frac{5t^3 - t^2 - t}{\sqrt{6t+3}}\, dt = \frac{1}{35(3+\sqrt{3})}.$$

Appendix B Connection between discrete and continuous coarsening laws

Here we show that the discrete coarsening law (3.10) can be recovered back from (3.14) if the initial distribution $f(x)$ has the form (3.15), i.e. if it is represented by $k \in \mathbb{N}$ families as in (3.7), where we denote

$$i'_m = \lim_{N\to\infty} \frac{i_m}{N}.$$

In this case (3.13) implies

$$n(d) = 1 - \sum_{p=m}^{k} i'_m \quad \text{if} \quad d \in [d_m, d_{m-1}).$$

Substituting the last expression in (3.14) implies

$$BT(d_m) = d_k \ln\left[\frac{1}{1-\sum_{p=m}^k i'_m}\right] + (d_{k-1} - d_k)\ln\left[\frac{1-i'_k}{1-\sum_{p=m}^k i'_m}\right] + \cdots$$
$$+ (d_{m+1} - d_m)\ln\left[\frac{1-\sum_{p=m+1}^k i'_m}{1-\sum_{p=m}^k i'_m}\right] = BT(h_{m+1})$$
$$+ \left(Nd_m + \sum_{p=m}^{k}(d_p - d_m)i_p\right)\ln\left[\frac{1-\sum_{p=m+1}^k i'_m}{1-\sum_{p=m}^k i'_m}\right].$$

Therefore, one obtains recursively that

$$T(d_m) = \sum_{p=m}^{k} \frac{1}{B}\left(Nd_p + \sum_{p'=p}^{k}(d'_p - d_p)i'_p\right)\ln\left[\frac{1-\sum_{p=m+1}^k i'_m}{1-\sum_{p=m}^k i'_m}\right]. \tag{B 1}$$

On the other hand, dividing (3.10) by N and proceeding to the limit $N \to \infty$ with k fixed, one obtains exactly (B 1).

https://doi.org/10.1017/S0956792513000314 Published online by Cambridge University Press

References

[1] Bates, P. W. & Xun, J. P. (1994) Metastable patterns for the Cahn-Hilliard equation: Part I. *J. Diff. Equ.* **111**, 421–457.

[2] Bates, P. W. & Xun, J. P. (1995) Metastable patterns for the Cahn-Hilliard equation: Part II. Layer dynamics and slow invariant manifold. *J. Diff. Equ.* **117**, 165–216.

[3] Bertozzi, A. L., Grün, G. & Witelski, T. P. (2001) Dewetting films: Bifurcations and concentrations. *Nonlinearity* **14**, 1569–1592.

[4] Bonn, D., Eggers, J., Indekeu, J., Meunier, J. & Rolley, E. (2009) Wetting and spreading. *Rev. Mod. Phys.* **81**(2), 739.

[5] Bray, A. J. (1994) Theory of phase-ordering kinetics. *Adv. Phys.* **43**, 357–459.

[6] Brochard-Wyart, F., de Gennes, P.-G., Hervert, H. & Redon, C. (1994) Wetting and slippage of polymer melts on semi-ideal surfaces. *Langmuir* **10**, 1566–1572.

[7] Brochard-Wyart, F., Gay, C. & de Gennes, P. G. (1996) Slippage of polymer melts on grafted surfaces. *Macromolecules* **29**, 377–382.

[8] Brochard-Wyart, F. & Redon, C. (1992) Dynamics of liquid rim instabilities. *Langmuir* **8**, 2324–2329.

[9] Clasen, C., Eggers, E., Fontelos, M., Lie, J. & McKinley, G. H. (2006) The beads-on-string structure of viscoelastic threads. *J. Fluid Mech.* **556**, 283–308.

[10] Craster, R. V. & Matar, O. K. (2009) Dynamics and stability of thin liquid films. *Rev. Mod. Phys.* **81**(3), 1131.

[11] de Gennes, P. G. (1985) Wetting: Statics and dynamics. *Rev. Mod. Phys.* **57**, 827–863.

[12] Derrida, B., Godrèche, C. & Yekutieli, I. (1991) Scale-invariant regimes in one-dimensional models of growing and coalescing droplets. *Phys. Rev. A* **44**(10), 6241–6251.

[13] Erneux, T. & Davis, S. H. (1993) Nonlinear rupture of free films. *Phys. Fluids* **5**, 1117.

[14] Erneux, T. & Gallez, D. (1997) Can repulsive forces lead to stable patterns in thin liquid films? *Phys. Fluids* **9**, 1194–1196.

[15] Fetzer, R., Münch, A., Wagner, B., Rauscher, M. & Jacobs, K. (2007) Quantifying hydrodynamic slip: A comprehensive analysis of dewetting profiles. *Langmuir* **23**, 10559–10566.

[16] Glasner, K. B. (2008) Ostwald ripening in thin film equations. *SIAM J. Appl. Math.* **69**, 473–493.

[17] Glasner, K., Otto, F., Rump, T. & Slepjev, D. (2009) Ostwald ripening of droplets: The role of migration. *Eur. J. Appl. Math.* **20**(1), 1–67.

[18] Glasner, K. B. & Witelski, T. P. (2003) Coarsening dynamics of dewetting films. *Phys. Rev. E* **67**, 016302.

[19] Glasner, K. B. & Witelski, T. P. (2005) Collission vs. collapse of droplets in coarsening of dewetting thin films. *Physica D* **209**, 80–104.

[20] Kargupta, K., Sharma, A. & Khanna, R. (2004) Instability, dynamics and morphology of thin slipping films. *Langmuir* **20**, 244–253.

[21] Kitavtsev, G. (2009) *Derivation, Analysis and Numerics of Reduced Ode Models Describing Coarsening Dynamics of Liquid Droplets*. PhD thesis, Institute of Mathematics, Humboldt University of Berlin, Berlin, Germany.

[22] Kitavtsev, G., Laurençot, P. & Niethammer, B. (2011) Weak solutions to lubrication equations in the presence of strong slippage. *Methods Appl. Anal.* **18**, 183–202.

[23] Kitavtsev, G., Recke, L. & Wagner, B. (2011) Center manifold reduction approach for the lubrication equation. *Nonlinearity* **24**(8), 2347–2369.

[24] Kitavtsev, G. & Wagner, B. (2010) Coarsening dynamics of slipping droplets. *J. Engr. Math.* **66**, 271–292.

[25] Limary, R. & Green, P. F. (2002) Late-stage coarsening of an unstable structured liquid film. *Phys. Rev. E* **60**, 021601.

[26] Limary, R. & Green, P. F. (2003) Dynamics of droplets on the surface of a structured fluid film: Late-stage coarsening. *Langmuir* **19**, 2419–2424.

[27] Menon, G., Niethammer, B. & Pego, B. (2010) Dynamics and self-similarity in min-driven clustering. *Trans. Amer. Math. Soc.* **362**, 6591–6618.
[28] Menon, G. & Pego, B. (2004) Approach to self-similarity in Smoluchowskis coagulation equations. *Comm. Pure Appl. Math.* **57**(9), 1197–1232.
[29] Menon, G. & Pego, B. (2008) The scaling attractor and ultimate dynamics for Smoluchowskis coagulation equations. *J. Nonlinear Sci.* **18**(2), 143–190.
[30] Münch, A. (2005) Dewetting rates of thin liquid films. *J. Phys. Condens. Matter* **17**, S309–S318.
[31] Münch, A. & Wagner, B. (2005) Contact-line instability of dewetting thin films. *Physica D* **209**, 178–190.
[32] Münch, A., Wagner, B. & Witelski, T. P. (2006) Lubrication models with small to large slip lengths. *J. Engr. Math.* **53**, 359–383.
[33] Oron, A., Davis, S. H. & Bankoff, S. G. (1997) Long-scale evolution of thin liquid films. *Rev. Mod. Phys.* **69**(3), 931–980.
[34] Otto, F., Rump, T. & Slepjev, D. (2006) Coarsening rates for a droplet model: Rigorous upper bounds. *SIAM J. Appl. Math.* **38**, 503–529.
[35] Peschka, D. (2008) *Self-Similar Rupture of Thin Liquid Films With Slippage*. PhD thesis, Institute of Mathematics, Humboldt University of Berlin, Berlin, Germany.
[36] Pismen, L. M. & Pomeau, Y. (2004) Mobility and interactions of weakly nonwetting droplets. *Phys. Fluids* **16**, 2604–2612.
[37] Redon, C., Brochard-Wyart, F. & Rondelez, F. (1991) Dynamics of dewetting. *Phys. Rev. Lett.* **66**(6), 715–718.
[38] Reiter, G., Sharma, A., Casoli, A., David, M.-O., Khanna, R. & Auroy, P. (1999) Thin film instability induced by long range forces. *Langmuir* **15**, 2551–2558.
[39] San, X. & Ward, M. J. (2000) Dynamics and coarsening of interfaces for the viscous Cahn–Hilliard equation in one spatial dimension. *Stud. Appl. Math.* **105**, 203–234.
[40] Seemann, R., Herminghaus, S. & Jacobs, K. (2001) Gaining control of pattern formation of dewetting films. *J. Phys. Condens. Matter* **13**, 4925–4938.
[41] Sharma, A. & Reiter, G. (1996) Instability of thin polymer films on coated substrates: Rupture, dewetting and drop formation. *J. Colloid Interface Sci.* **178**, 383–389.
[42] Williams, M. B. & Davis, S. H. (1982) Nonlinear theory of film rupture. *J. Colloid Interface Sci.* **90**, 220–228.